

CONSTRAINING Ω_0 WITH THE ANGULAR SIZE–REDSHIFT RELATION OF DOUBLE-LOBED QUASARS IN THE FIRST SURVEY

ARI BUCHALTER,^{1,2} DAVID J. HELFAND,^{1,3} ROBERT H. BECKER,^{4,5} AND RICHARD L. WHITE^{6,7}

Received 1997 June 13; accepted 1997 September 29

ABSTRACT

In previous attempts to measure cosmological parameters from the angular size–redshift (θ - z) relation of double-lobed radio sources, the observed data have generally been consistent with a static Euclidean universe rather than with standard Friedmann models, and past authors have disagreed significantly as to what effects are responsible for this observation. These results and different interpretations may be due largely to a variety of selection effects and differences in the sample definitions destroying the integrity of the data sets, and inconsistencies in the analysis undermining the results. Using the VLA FIRST survey, we investigate the θ - z relation for a new sample of double-lobed quasars. We define a set of 103 sources, carefully addressing the various potential problems that, we believe, have compromised past work, including a robust definition of size and the completeness and homogeneity of the sample, and further devise a self-consistent method to assure accurate morphological classification and account for finite resolution effects in the analysis. Before focusing on cosmological constraints, we investigate the possible impact of correlations among the intrinsic properties of these sources over the entire assumed range of allowed cosmological parameter values. For all cases, we find apparent size evolution of the form $l \propto (1+z)^c$, with $c \approx -0.8 \pm 0.4$, which is found to arise mainly from a power-size correlation of the form $l \propto P^\beta$ ($\beta \approx -0.13 \pm 0.06$) coupled with a power-redshift correlation. Intrinsic size evolution is consistent with zero. We also find that in all cases, a subsample with $c \approx 0$ can be defined, whose θ - z relation should therefore arise primarily from cosmological effects. These results are found to be independent of orientation effects, although other evidence indicates that orientation effects are present and consistent with predictions of the unified scheme for radio-loud active galactic nuclei. The above results are all confirmed by nonparametric analysis.

Contrary to past work, we find that the observed θ - z relation for our sample is more consistent with standard Friedmann models than with a static Euclidean universe. Though the current data cannot distinguish with high significance between various Friedmann models, significant constraints on the cosmological parameters within a given model are obtained. In particular, we find that a flat, matter-dominated universe ($\Omega_0 = 1$), a flat universe with a cosmological constant, and an open universe all provide comparably good fits to the data, with the latter two models both yielding $\Omega_0 \approx 0.35$ with 1σ ranges including values between ~ 0.25 and 1.0 ; the $c \approx 0$ subsamples yield values of Ω_0 near unity in these models, though with even greater error ranges. We also examine the values of H_0 implied by the data, using plausible assumptions about the intrinsic source sizes, and find these to be consistent with the currently accepted range of values. We determine the sample size needed to improve significantly the results and outline future strategies for such work.

Subject headings: cosmology: observations — galaxies: fundamental parameters — quasars: general — radio continuum: galaxies

1. INTRODUCTION

The angular size–redshift (θ - z) relation for a cosmological population of standard rods is a powerful probe of the large-scale geometry of the universe. For a universe characterized by the Friedmann-Robertson-Walker metric, with curvature arising from the energy density of ordinary matter, and possibly a cosmological constant, the angular size of a rod of intrinsic length l , viewed at an angle ϕ to the line of sight is given by

$$\theta = \frac{l \sin \phi}{D_A}, \quad D_A = \frac{cR_0}{1+z} \sum \left(\int_1^{1+z} \frac{dx}{H_0 R_0 [\Omega_0 x^3 + (1 - \Omega_0 - \Omega_\Lambda)x^2 + \Omega_\Lambda]^{1/2}} \right) \quad (1)$$

(Weinberg 1972), where D_A is the angular-size distance, H_0 is the present value of the Hubble constant, R_0 is the expansion scale factor in units of time, c is the speed of light, Ω_0 is the present ratio of the matter density to the critical density, $\Omega_\Lambda = \Lambda/3H_0^2$ (where Λ is the cosmological constant), and $\Sigma(x) = \sin x$, x , $\sinh x$ for closed, flat, and open geometries, respectively. Contributions to the energy density arising from more exotic phenomena such as textures will affect the angular

¹ Department of Astronomy, Columbia University, New York, NY 10027.

² ari@astro.columbia.edu.

³ djh@astro.columbia.edu.

⁴ Department of Physics, University of California, Davis, CA 95616; and IGPP/Lawrence Livermore National Laboratory.

⁵ bob@igpp.llnl.gov.

⁶ Space Telescope Science Institute, 3700 San Martin Drive, Baltimore, MD 21218.

⁷ rlw@stsci.edu.

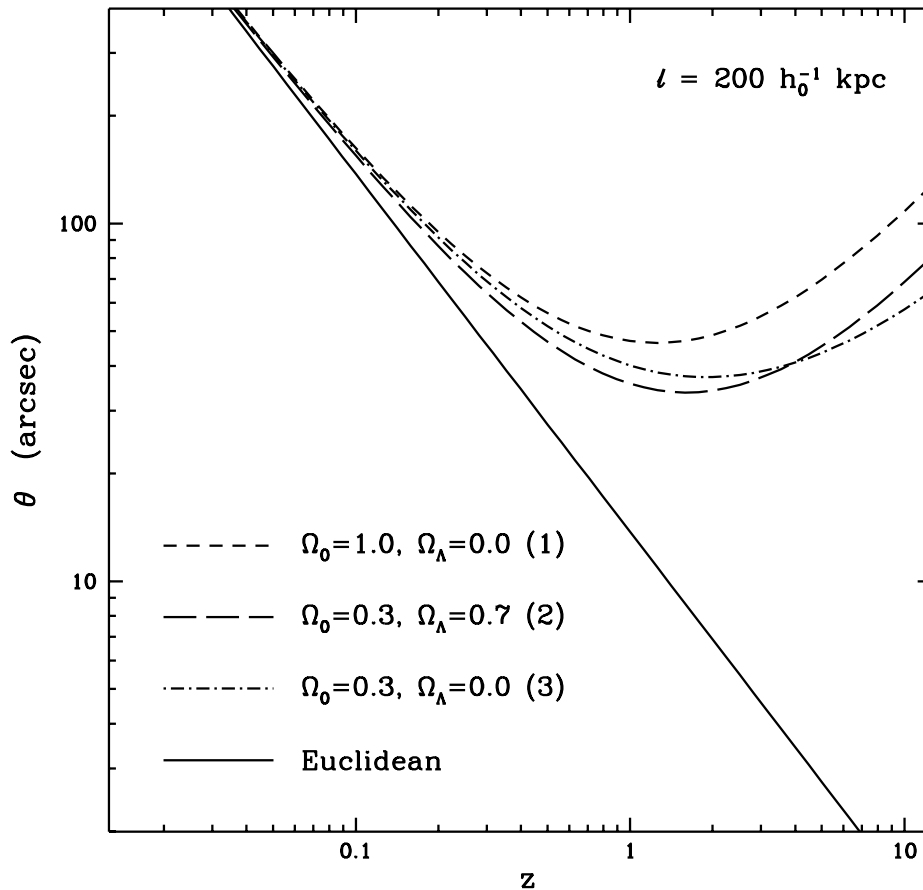


FIG. 1.—The θ - z relation for deprojected rods of length $200 h_0^{-1}$ kpc for different cosmologies. The choices for Ω_0 and Ω_Λ in the three Friedmann models (denoted in parentheses) are listed on the figure. The curve for a static Euclidean universe is shown for comparison. In practice, the curves actually define upper limits to the observed angular sizes, since projection effects will scatter the observed sizes downward. Note the presence of the minimum near $z \sim 1.5$ in the Friedmann models.

size in a straightforward manner but are not considered here. Figure 1 illustrates the θ - z relation for deprojected rods ($\phi = 90^\circ$) with an intrinsic size of $l = 200 h_0^{-1}$ kpc (h_0 is the Hubble constant in units of $100 \text{ km s}^{-1} \text{ Mpc}^{-1}$) for three Friedmann cosmologies: (1) an Einstein-de Sitter universe with $\Omega_0 \equiv 1$ and $\Omega_\Lambda = 0$; (2) a flat universe with $0 < \Omega_0 \leq 1$, $\Omega_0 + \Omega_\Lambda = 1$; and (3) a nonclosed, matter-dominated universe with $0 < \Omega_0 \leq 1$, $\Omega_\Lambda = 0$ (we will hereafter refer to these as models 1, 2, and 3, respectively). Model 1 is, in effect, a limiting case of models 2 and 3, and we do not consider models with $\Omega_0 > 1$. The particular values chosen for Ω_0 and Ω_Λ in the figure are listed, and the curve for a static Euclidean universe, with $\theta \propto z^{-1}$ (hereafter referred to simply as the Euclidean model), is shown for comparison. The amplitudes of the Friedmann curves are scaled by h_0 , while their shapes and, in particular, the location of the minimum in the angular size (typically between $z = 1$ and $z = 2$) depend on Ω_0 and Ω_Λ . For randomly oriented rods, these curves actually define upper limits to the observed angular size distribution, since projection effects will scatter the observed sizes downward. Note that for the conventional parameter values listed in Figure 1, the curves for the different Friedmann models, particularly the underdense (Ω_0 possibly less than 1) models 2 and 3, are fairly similar.

With the discovery of double-lobed radio galaxies and quasars, it was hoped that a standard rod had been found that could constitute a useful high-redshift sample for measuring the geometry of the universe. Early work (Miley 1971; Wardle & Miley 1974; Hooley et al. 1978) revealed, however, that the upper limit to the θ - z data traced a Euclidean curve, implying that some effect must be diminishing the apparent sizes of these objects at high redshift. Subsequent studies (Kapahi 1985, 1989; Singal 1988, 1993; Barthel & Miley 1988; Onuora 1989; Ubachukwu & Onuora 1993; Nilsson et al. 1993; Chyży & Zięba 1993), looking at the variation of binned mean or median angular sizes as a function of redshift to compensate for projection effects, all confirmed that the observed θ - z data was strikingly consistent with a Euclidean model.

Three main explanations have been proposed to account for this observation: (1) The characteristic length scale of double-lobed sources may change with cosmic epoch, presumably due to differences in the density of the intergalactic medium (IGM) and/or changes in the energetics of the active galactic nuclei (AGN) that power these sources. Intrinsic size evolution of the form $l \propto (1+z)^n$, with $n < 0$ so that higher redshift objects are intrinsically smaller, would reconcile the data with Friedmann models. (2) Since power, P , and redshift are necessarily correlated in any flux-limited sample, usually approximated by $P \propto (1+z)^x$, a negative correlation between power and intrinsic size, typically parameterized as $l \propto P^\beta$, with $\beta < 0$, would give rise to an apparent correlation between l and z , given by $l \propto (1+z)^{\beta x}$, effectively mimicking size evolution. In general, effects 1 and 2 may both be present, giving rise to overall observed size evolution of the form $(1+z)^c$, where $c = \beta x + n$ (Ubachukwu 1995). (3) According to the unified model for radio sources, the classification of an object as a radio

galaxy or a quasar depends only on its orientation, with quasars having inclinations within about 45° of the line of sight, with a median inclination of 31° , and radio galaxies being inclined roughly between 45° and 90° , with a median inclination of 69° (Barthel 1989; Lister et al. 1994). If the unified scheme is correct, then in studies that include both radio galaxies and quasars, the high-redshift population (dominated by quasars) would have systematically smaller mean angular sizes than the low-redshift population (dominated by radio galaxies), making the universe appear more Euclidean. A similar scheme has been proposed to unify the two classes of radio-loud quasars, the core-dominated and lobe-dominated quasars (CDQs and LDQs) (Orr & Browne 1982), assuming that only the radio flux from the compact core is relativistically beamed. In this model, the moderately beamed LDQs, with a median ratio of the core-to-lobe flux density, $R \sim 0.1$, have a median inclination of 40° to the line of sight, while the more strongly beamed CDQs, with a median $R \sim 10$, have a median inclination of 10° (Hough & Readhead 1989; Ubachukwu 1996). If the observed fraction of CDQs increases with redshift, as might be expected in a flux-limited sample, then even studies limited to quasar samples would also reveal a deficit of larger sources at higher redshifts.

While most previous studies agree that the observed data follow a Euclidean trend, they disagree substantially as to what combination of the above effects is responsible. Several authors find evidence for significant size evolution (Kapahi 1985; Oort et al. 1987; Barthel & Miley 1988; Kapahi 1989; Neeser et al. 1995), while others claim to find an l - P correlation with little or no intrinsic size evolution (Hooley et al. 1978; Masson 1980; Onuora 1991; Chyży & Zięba 1993; Nilsson et al. 1993). Moreover, there has been considerable disagreement as to whether the properties of radio galaxies and quasars follow similar trends. Some authors find evidence for stronger size evolution in the double-lobed radio galaxy population (Onuora 1989; Chyży & Zięba 1993; Singal 1993) than in the double-lobed quasar population, while several workers have found a negative l - P correlation for quasars but a positive one for radio galaxies (Chyży & Zięba 1993; Nilsson et al. 1993; Singal 1993). Others have claimed to see identical trends in the two populations (Gopal-Krishna & Kulkarni 1992) and even to reconcile the observed θ - z data with Friedmann cosmologies based on orientation effects within the unified scheme (Onuora 1991).

The lack of concordance among these previous results strongly suggests that the construction and analysis of samples of double-lobed objects has been dominated by systematic and/or selection effects that are unrelated to the intrinsic behavior of the sources. In fact, several investigations have traced the inconsistent results of various studies to such selection effects (Neeser et al. 1995) or to different sample definitions (Nilsson et al. 1993). We believe that other substantive issues have not been properly incorporated into the study of the θ - z relation for double-lobed sources and have also compromised the results. We summarize these issues below:

1. In determining the morphological properties of double-lobed sources, it is desirable to characterize each source using parameters that make no a priori assumptions about the source structure and are related as directly as possible to the measured data. The moments of the brightness distribution, $B(\vartheta)$, where ϑ represents two-dimensional, quasi-Cartesian coordinates, form one such set of parameters (Burn & Conway 1976). In particular, the second moment, $\theta_{sm} = 2[\int \vartheta^2 B(\vartheta) d\vartheta / \int B(\vartheta) d\vartheta]^{1/2}$, is a model-independent measure of the source size that, for sufficiently large sources ($\gtrsim \frac{1}{3}$ of the beam), is independent of the beam resolution (Condon 1988; P. H. Coleman 1996, private communication). For double-lobed sources, however, θ_{sm} is an unstable diagnostic since it is a flux-weighted quantity; two sources with identical lobe structures (i.e., apparent shapes, sizes, and lobe-lobe separation) would yield a different value of θ_{sm} (a) if one exhibited a significant core component (e.g., because it was an intrinsically large source with its core flux relativistically boosted by projection, as opposed to a smaller, deprojected source with the same apparent lobe properties but no detected core flux), (b) if the ratio of the lobe fluxes in the two sources differed, or (c) if the maps of the two source fields had different signal-to-noise properties. In addition, surveys with different flux sensitivities and limiting resolutions can yield different values of θ_{sm} for the same source. The more commonly used measure of the angular size of double-lobed sources is the “largest angular size” (LAS), typically taken to be either the maximum linear extent over which a given level of radio emission is detected, θ_{max} , or the peak-to-peak angular separation, θ_{pp} . The former definition, however, is also a poor measure of size since it is highly sensitive to the details of the observation; radio observations conducted with different instruments at different frequencies, with different flux sensitivities and beamwidths, can yield drastically different values of θ_{max} for the same object. An example of this is illustrated in Neeser et al. (1993). Even within a given radio data set, the measured value of θ_{max} for an arbitrary distribution of high-redshift, extended objects is highly susceptible to the effects of cosmological surface brightness dimming.

For these reasons, many authors studying the θ - z relation for double-lobed sources focus on Fanaroff-Riley type II (FR-II) objects (Fanaroff & Riley 1974), which exhibit radio-bright hot-spots near the outer edges of the lobes. For these objects, the peak-to-peak size is largely independent of the details of the observation and thus provides a fairly robust measure of the angular size (see § 2 for further discussion).⁸ However, the peak positions, and thus peak-to-peak sizes, are typically derived from fitting a specific model (usually Gaussians) to the brightness distribution of each source. Fitting Gaussians to the highly asymmetric, edge-brightened lobe components of FR-IIIs will necessarily return peak positions that are slightly closer to the

⁸ Though θ_{pp} is fairly insensitive to details of the observation, it may be asked whether the hot spots in different FR-II sources occur at the same relative positions, so that one is in fact measuring a stable quantity for different sources. The canonical criterion for FR-II sources is that the ratio, $FR = \theta_{pp}/\theta_{max}$, where θ_{max} is defined as the greatest linear extent of the outer lobes measured to the 1% contour, be greater than 0.5. Though θ_{max} may generally depend on the details of the observation, studies have shown that FR-IIIs invariably tend to have FR values near unity. Rector, Stocke, & Ellingson (1995) study a sample of 30 FR-IIIs in the range $0.26 < z < 0.63$ and find, for those with well-determined values of FR, a mean FR value of 0.85 with a standard deviation of 0.07, with all having $FR > 0.7$. Thus, the relative peak-to-peak scales in these sources vary by at most 17% from the mean value, although typically much less, and show no systematic variation with redshift. It should be noted that the spread in FR may arise from the fact that if the lobes themselves are not spherically symmetric, FR will vary simply because the apparent location of the hot spots within the optically thin lobes will vary for sources with different projection angles, even if the relative positions of the hot spots within the lobes of these sources are identical, suggesting that θ_{pp} is in fact a more stable quantity than FR. The variation in FR may also be due in part to instrumental effects and/or cosmological surface brightness dimming operating in the determination of θ_{max} , rather than intrinsic differences in θ_{pp} .

central core and, thus, will *underestimate* the peak-to-peak angular size. The resulting fractional error in the angular size would be small for large sources, but it may be appreciable for smaller sources where the resolved lobe size is comparable to the angular distance between lobes. For small enough sources, standard Gaussian fitting routines may fit only one or two components to a source that clearly exhibits a more complicated morphology and thus drastically underestimate θ_{pp} . These effects would become most pronounced at higher redshifts ($0.5 \lesssim z \lesssim 3.0$), where the relative fraction of smaller sources is greatest (cf. Fig. 1), and precisely where cosmological effects in the θ - z plane become important, thus making the universe appear more Euclidean at higher redshifts. It is preferable therefore to measure θ_{pp} for FR-II sources directly from the radio data of a single, high-resolution survey, rather than from multiple survey catalogs generated by model-specific fitting algorithms. Despite these considerations, most of the θ - z studies to date have, in fact, employed samples compiled from output catalogs of multiple radio surveys (Miley 1971; Hooley et al. 1978; Singal 1988, 1993; Kapahi 1989; Nilsson et al. 1993; Neeser et al. 1995). A further danger in using data taken from multiple surveys is that such a study may selectively omit some sources altogether. For example, large, low surface brightness objects detected in a low-resolution sample may be resolved out in a deep, high-resolution sample, and a high-frequency sample will generally contain more compact sources than a low-frequency sample. The mixing of sources from different samples may thus destroy the consistency of the set required to measure the θ - z relation.

2. The sizes of double-lobed sources are measured from radio data, but the redshift information is often obtained in an optically selected fashion. Thus, constructing a θ - z diagram from quasar catalogs (as all previous studies have done) might mix radio-measured angular sizes with optically selected redshifts and may introduce serious selection effects. Although one may hope that the highly heterogeneous manner in which lists of quasar redshifts have been developed would “wash out” any such effects, it is easy to conceive of scenarios wherein the sizes of an optically selected subset of double-lobed radio objects could be systematically larger or smaller than the population as a whole. Such a selection effect, if present, would operate even when using catalogs with complete optical identifications and redshift information. To eliminate this potential problem would require obtaining redshift information for a complete set of *radio-selected* double-lobed objects, but such a θ - z study has not been carried out to date.

3. For the purposes of studying cosmology using the θ - z relation, double-lobed sources are chosen to the extent that they might represent a population of standard rods. It is clear, however, that a given double-lobed source does not maintain a fixed size, but rather, grows with time, over a period of roughly 10^7 – 10^8 yr (Gopal-Krishna et al. 1996) (This growth is not to be confused with the intrinsic size evolution discussed above, which occurs over cosmological time frames and refers to evolution of the overall length scale characterizing these objects and not the growth in size of a given source.) Thus, when considering the angular sizes of these sources, those with smaller sizes will in general be a mixture of intrinsically smaller sources plus larger sources viewed in projection. Moreover, many radio sources exhibit a core-jet structure that, if not well-resolved, can easily be mistaken for a small double-lobed morphology, and many small, double-lobed sources may not be sufficiently resolved for an accurate classification. To avoid potential confusion, it is necessary to determine, for a given set of radio observations, the angular scale above which morphological classifications can be accurately determined. This scale will generally be significantly greater than the survey resolution limit. However, previous θ - z studies include angular sizes down to the survey resolution limits (Barthel & Miley 1988; Singal 1988, 1993; Nilsson et al. 1993; Neeser et al. 1995) and are thus mixing true double-lobed sources of various sizes together with objects that may in fact be a different class of sources, and by using multiple surveys, are doing so in a highly nonuniform fashion. The resulting admixture of objects is not likely to yield a good approximation to a standard rod, and while interesting from the viewpoint of AGN evolution, is not valid for cosmological studies. Since the morphologies of objects with large angular sizes are less likely to be misclassified, this problem also becomes more severe at higher redshifts, where there is a greater fraction of smaller, less well-resolved sources. The wrongful inclusion of more smaller sources at higher redshifts would significantly *decrease* the mean angular size at these redshifts, again making the universe appear more Euclidean.

4. Another important consequence of finite survey resolution is that a constant angular resolution limit does not correspond to a constant minimum linear size, but rather one that varies with redshift (cf. eq. [1] and Fig. 1). Thus, if all the θ - z data down to some limiting resolution are used, the resulting sample not only will mix sources with different intrinsic sizes (due to the spread in the intrinsic size distribution) but will span different ranges of intrinsic sizes at different redshifts. This redshift dependence of the intrinsic size distribution again undermines the consistency needed to define a cosmological population of standard rods.

The VLA FIRST Survey (Becker, White, & Helfand 1995) is the most sensitive survey of its kind, and represents a valuable new tool for studying the θ - z relation. To date, the project has mapped ~ 3000 deg² of the north Galactic cap at 1.4 GHz to a sensitivity of ~ 1 mJy with a $5''.4$ FWHM Gaussian beam and has cataloged roughly 270,000 sources with subarcsecond positional accuracy. In this paper we investigate the θ - z relation for double-lobed quasars in the FIRST survey. We construct a sample optimally suited for studying the θ - z relation, addressing the various problems and selection effects that may be present, and devise analytic methods to account for these (§ 2). In § 3, we explore the relationships among the intrinsic properties of the sources, using both parametric and nonparametric methods, and find evidence, regardless of the chosen cosmological parameters, for a negative correlation between power and size, with $\beta \approx -0.13 \pm 0.06$, which, coupled with the observed power-redshift correlation, gives rise to apparent size evolution with $c \approx -0.8 \pm 0.4$; intrinsic size evolution is consistent with zero. We also find that a subsample can be defined for which c is consistent with zero, implying that any observed θ - z relation would be entirely due to cosmological effects. We find these results to be independent of orientation effects, although other evidence confirms that orientation effects are present and consistent with the predictions of the unified scheme for radio-loud AGNs. In § 4, we investigate the constraints that can be placed on cosmological parameters from the θ - z data and find that, contrary to past work, the observed data are less consistent with a Euclidean model than with standard Friedmann models. Both underdense models yield $\Omega_0 \approx 0.35$, with 1σ intervals ranging from ~ 0.25 to 1.0, and the $c \approx 0$

subsample favors values near unity in these models. Model 1, with $\Omega_0 \equiv 1$, provides a comparably good fit and even appears slightly favored by the $c \approx 0$ subsample, although these results are likely due to the reduced number of free parameters in this model. Although all three Friedmann models yield consistent values of Ω_0 , the data at present cannot distinguish between different cosmological models with reasonable significance. As a consistency check on our analysis, we also investigate the values of H_0 implied by the data, based on assumptions about the intrinsic sizes of the sources, and find the results to be consistent with the range spanned by current estimates. In § 5 we present our conclusions and discuss future prospects for such work.

2. THE SAMPLE

2.1. Selection Criteria

In the interest of maintaining a maximally homogeneous population of objects, we restrict our study of double-lobed sources to those identified as quasars, excluding objects classified as radio galaxies. We thus bypass the issue of whether the potentially different characteristics of these two kinds of objects, such as different mean orientations or power-size correlations, produce noncosmological effects in the θ - z plane. Moreover, since all Friedmann models approach a Euclidean universe as $z \rightarrow 0$ (see Fig. 1), the low-redshift population (dominated by radio galaxies) carries less information about the cosmology. Conversely, since many quasars are found at higher redshifts ($z \gtrsim 1$), where the predictions of different models exhibit different minima and begin to diverge significantly, their θ - z distribution is more sensitive to Ω_0 and Ω_Λ . In addition, we further restricted our sample to sources with $z > 0.3$, since, as mentioned in § 1, past work indicates that the properties of low- z and high- z radio sources exhibit different behaviors, with the cutoff occurring roughly at $z = 0.3$, beyond which quasars begin to dominate (Heckman et al. 1992; Hes et al. 1995).

Using the Hewitt & Burbidge (1993), Veron-Cetty & Veron (1996), and FIRST Bright QSO Survey (Gregg et al. 1996; R. H. Becker et al. 1997, private communication) catalogs, we selected all $z > 0.3$ quasars whose positions fell within the currently mapped area of the FIRST survey. Each of these was then inspected separately by A. B. and C. T. W.⁹ on the FIRST radio maps to determine the radio morphology. We included in our sample only those sources where the quasar position fell near (i.e., within a few arcseconds of) the center of an edge-brightened, double-lobed radio source. Restricting the study to edge-brightened, FR-II objects offers two main advantages. First, since the lobes have radio-bright hot spots, the measured peak-to-peak angular sizes are less sensitive to instrumental effects and cosmological surface brightness dimming (Neeser et al. 1995) than are FR-I sources, whose lobe components fade gradually toward the edges. Second, since the underlying mechanism that distinguishes FR-I and FR-II sources is not well understood, restricting the analysis to a single type of object assures us that the θ - z data are not altered by noncosmological effects that may arise from intrinsic differences between these objects. Determining the radio morphology (i.e., FR-I, FR-II, core-jet, etc.) is relatively easy for sources significantly larger than the beam but can be problematic for smaller sources, either because of the limited survey resolution or because uncertainties in the optical positions of the quasars make it difficult to determine whether the radio peak corresponds to a core or a lobe. It is unlikely that FR-I sources would be misclassified as FR-IIs; cosmological surface brightness dimming would select against very faint FR-Is with $z > 0.3$, and recent studies have shown that there is a real decline in the incidence of powerful FR-Is with redshift (with few having $z > 0.3$), while the number of FR-IIs increases with redshift (Zirbel 1996). Following Neeser et al. (1995), we classify smaller sources as FR-II only if the quasar position is at the center of two comparable edge-brightened lobes, excluding sources that suggested a core-jet morphology, such as those where the quasar position falls much closer to one of the components or those where one component is much brighter than the other. Sources too small for an accurate morphological classification were omitted, thus introducing an effective size cutoff in the data, the significance of which is described in § 2.3. We excluded from our sample any sources with highly distorted or bent morphologies, whose apparent sizes have been severely influenced by asymmetric interaction with the IGM.

2.2. Properties of the Sample

A total of 103 objects satisfied our selection criteria. For each object we measured the peak-to-peak angular size, hereafter denoted simply by θ , directly from the FIRST radio maps, so as to avoid any systematic underestimation of the sizes that could arise from using the peaks of the Gaussian model fits. We also recorded the FIRST flux density for each source component; for components that are well resolved, such as the compact core components or sufficiently small lobe components, the measured FIRST fluxes are reliable. However, because of its high resolution, the FIRST survey is prone to resolving out flux from extended sources, such as the radio lobes of larger FR-IIs. Thus we also measured, where possible, the 1.4 GHz flux densities for our sources from the NRAO VLA Sky Survey (NVSS) radio survey (Condon et al. 1996), which is currently mapping 82% of the celestial sphere at 1.4 GHz to a sensitivity of 2.5 mJy with 45' FWHM resolution. Any difference between the FIRST and NVSS fluxes for a given source was ascribed to the extended lobe components, so that the total flux density, S_t , corresponds to the value measured by the NVSS survey (if available), while the core flux density, if any, is determined by the FIRST measurement. Many sources do not have a core component in the FIRST catalog, either because none was detected or, in the case of smaller sources, because the Gaussian fitting algorithm did not generate a separate component for the core. The data for our sample are listed in Table 1. For comparative purposes, we also measured θ_{sm} (not shown) for each source using both the FIRST and NVSS radio data.

Figure 2 shows a scatter plot of the θ - z data. The errors in the measured values of θ are typically $\sim 1''$, far less than the scatter in the angular sizes at any redshift. For graphical purposes, we bin the data in redshift, both in equal intervals of

⁹ We thank Chelsea T. Wald for her work in analyzing the radio images.

TABLE 1
DOUBLE-LOBED RADIO QUASAR DATA

α (J2000)	δ (J2000)	z	θ (arcsec)	S_r (mJy)	S_l (mJy)	R	Reference
00 22 44.3.....	-01 45 51	0.691	85.7	242.2	232.7	0.04	1
00 41 25.9.....	-01 43 15	1.679	19.3	1042.1	1042.1	0.00	1
01 03 29.4.....	+00 40 54	1.436	26.3	114.7	114.7	0.00	1
01 19 10.0.....	+01 31 28	0.520	84.2	60.3	58.1	0.04	4
01 33 52.7.....	+01 13 46	1.370	100.5	109.9	93.2	0.18	1
02 10 08.5.....	+01 18 39	0.870	154.4	33.6	27.0	0.24	4
02 25 07.9.....	-00 35 32	0.687	12.5	1141.4	1141.4	0.00	1
02 39 13.6.....	-01 18 16	1.794	15.1	237.5	237.5	0.00	1
02 45 34.0.....	+01 08 13	1.520	52.5	330.1	318.4	0.04	1
02 50 48.6.....	+00 02 08	0.766	16.5	111.1	91.3	0.22	1
03 15 42.4.....	-01 51 23	1.480	27.9	278.2 ^F	156.7	0.78	4
07 43 45.0.....	+23 28 39	0.770	23.6	335.1	181.1	0.85	1
07 45 41.6.....	+31 42 56	0.461	115.1	1454.7	840.0	0.73	1
07 52 28.7.....	+37 50 52	1.200	28.2	395.7	365.9	0.08	1
07 53 28.3.....	+33 50 52	2.070	27.3	150.3	87.2	0.72	1
08 02 20.5.....	+30 35 43	1.640	53.2	67.5	39.7	0.70	3
08 09 06.2.....	+29 12 35	1.470	131.4	312.9	291.4	0.07	3
08 11 36.9.....	+28 45 03	1.910	58.6	102.2	62.8	0.63	1
08 14 09.3.....	+32 37 31	0.842	24.2	514.5	387.6	0.33	1
08 14 30.6.....	+38 58 35	2.621	24.7	72.3	72.3	0.00	1
08 17 35.1.....	+22 37 17	0.980	23.6	1315.3	1150.5	0.14	1
08 17 40.2.....	+34 54 52	1.348	52.8	26.2	19.9	0.32	2
08 28 06.8.....	+39 35 40	0.762	64.6	86.7	81.6	0.06	1
08 32 36.7.....	+33 32 05	1.100	30.1	354.2	354.2	0.00	1
08 32 48.4.....	+42 24 59	1.051	16.1	456.1	168.7	1.70	1
08 46 59.3.....	+34 48 25	1.575	30.5	101.6	62.1	0.64	2
08 47 56.4.....	+31 47 58	1.834	161.1	1589.7	1568.0	0.01	1
08 52 34.2.....	+42 15 28	0.978	20.0	459.6	459.6	0.00	1
09 04 29.6.....	+28 19 33	1.121	22.5	130.1	90.9	0.43	1
09 07 45.5.....	+38 27 39	1.740	15.2	156.8	112.6	0.39	1
09 13 45.5.....	+40 56 27	0.442	20.6	16.4	8.1	1.02	1
09 13 52.4.....	+39 02 12	0.638	53.0	145.2	145.2	0.00	1
09 21 46.6.....	+37 54 10	1.108	51.9	825.0	547.0	0.51	1
09 25 54.7.....	+40 04 14	0.470	262.4	77.4	68.2	0.13	4
09 31 52.8.....	+34 39 20	2.304	12.8	26.6	18.8	0.42	2
09 37 04.0.....	+29 37 04	0.450	157.4	29.4	26.8	0.10	3
09 41 04.1.....	+38 53 51	0.618	51.1	668.6	443.8	0.51	1
09 52 31.9.....	+35 12 53	1.875	25.7	339.0	34.3	8.88	1
09 55 48.1.....	+35 33 23	1.241	18.8	522.7	522.7	0.00	1
09 58 02.8.....	+38 29 58	1.394	18.9	432.8	432.8	0.00	1
10 00 21.8.....	+22 33 19	0.419	34.1	1117.2	1117.2	0.00	1
10 04 45.8.....	+22 25 19	0.974	66.4	578.9 ^F	545.0	0.06	1
10 10 27.5.....	+41 32 38	0.612	31.8	1734.8	1394.5	0.24	1
10 14 35.8.....	+27 49 03	0.899	13.1	514.8	514.8	0.00	1
10 17 49.3.....	+27 32 05	0.469	21.1	1318.7	1318.7	0.00	1
10 18 25.5.....	+38 05 33	0.380	48.4	275.2	242.5	0.14	1
10 20 41.1.....	+39 58 11	0.830	159.9	9.6 ^F	9.6	0.00	4
10 21 17.5.....	+34 37 23	1.400	18.3	457.5	144.2	2.17	1
10 51 29.4.....	+23 48 02	1.274	15.4	485.2	485.2	0.00	1
10 52 50.1.....	+33 55 05	1.405	32.7	21.5	8.7	1.47	4
11 03 13.3.....	+30 14 43	0.380	73.1	167.5	59.8	1.80	1
11 07 26.8.....	+36 16 12	0.393	20.4	611.9 ^F	611.9	0.00	1
11 08 37.7.....	+38 58 41	0.781	67.1	877.7	867.8	0.01	1
11 10 40.2.....	+30 19 09	1.520	42.3	91.0	68.2	0.33	3
11 14 38.6.....	+40 37 20	0.734	13.3	3037.2	3037.2	0.00	1
11 19 03.2.....	+38 58 52	0.733	90.0	141.1	129.3	0.09	1
11 34 54.5.....	+30 05 26	0.614	15.1	1147.4	1147.4	0.00	1
11 48 18.8.....	+31 54 11	0.549	20.7	94.0	45.8	1.05	1
12 06 17.3.....	+38 12 35	0.838	35.1	241.0	241.0	0.00	1
12 10 37.7.....	+31 57 07	0.388	80.2	276.3	254.3	0.09	1
12 23 11.2.....	+37 07 02	0.489	36.0	477.3	430.1	0.11	1
12 30 52.5.....	+39 30 00	2.217	51.9	223.9	219.6	0.02	1
12 33 28.3.....	+34 39 42	0.847	31.0	41.8	33.9	0.23	2
12 36 31.3.....	+26 35 09	2.100	21.6	557.3	557.3	0.00	1
12 36 51.4.....	+25 07 48	0.546	83.8	270.6	254.4	0.06	1
12 37 04.0.....	+33 14 23	1.280	18.2	218.5	52.9	3.13	1
12 40 21.2.....	+35 02 59	1.194	16.8	222.1	222.1	0.00	1
12 47 20.7.....	+32 09 01	0.949	22.9	470.1	338.0	0.39	1
12 50 25.5.....	+30 16 40	1.061	28.6	430.6	430.6	0.00	1
12 54 10.5.....	+39 33 23	2.104	32.4	56.9	56.9	0.00	1
12 59 02.1.....	+39 00 13	0.978	20.9	297.1 ^F	258.1	0.15	1
13 00 33.4.....	+40 09 07	1.659	19.8	1287.2 ^F	1287.2	0.00	1

TABLE 1—*Continued*

α (J2000)	δ (J2000)	z	θ (arcsec)	S_1 (mJy)	S_l (mJy)	R	Reference
13 08 56.8.....	+27 08 12	1.537	15.2	334.6	180.2	0.86	1
13 41 08.2.....	+39 14 49	0.580	12.6	84.2	84.2	0.00	1
13 42 10.9.....	+28 28 47	0.330	94.6	224.2	222.7	0.01	1
13 42 54.5.....	+28 28 05	1.037	33.1	184.1	118.5	0.55	1
13 44 25.5.....	+38 41 29	1.533	18.8	286.9	286.9	0.00	1
13 50 15.0.....	+38 12 05	1.390	16.8	180.3	180.3	0.00	1
13 53 36.0.....	+26 31 48	0.310	173.2	244.5	222.2	0.10	1
14 11 55.3.....	+34 15 11	1.820	20.2	201.1	98.4	1.04	1
14 16 58.3.....	+34 28 53	0.750	14.8	151.1	151.1	0.00	1
14 25 50.8.....	+24 04 03	0.649	20.4	1479.5 ^F	1158.6	0.28	1
14 27 35.7.....	+26 32 14	0.366	228.4	368.5	314.4	0.17	1
14 37 56.5.....	+35 19 37	0.540	14.3	89.4	89.4	0.00	1
14 46 26.8.....	+41 33 18	0.675	102.9	534.1	531.1	0.01	1
15 14 43.0.....	+36 50 50	0.370	54.8	1001.2	930.2	0.08	1
15 57 30.0.....	+33 04 46	0.942	33.6	168.2	82.2	1.05	1
16 08 11.2.....	+28 49 02	1.989	30.3	589.5	570.5	0.03	1
16 13 51.4.....	+37 42 59	1.630	16.3	283.6	283.6	0.00	1
16 22 29.9.....	+35 31 26	1.473	21.9	381.6 ^F	351.2	0.09	1
16 24 22.1.....	+39 24 42	1.120	21.3	254.2	121.9	1.09	1
16 24 39.3.....	+23 45 12	0.927	22.7	2587.9 ^F	2171.9	0.19	1
16 25 30.8.....	+27 05 47	0.525	23.1	532.0	299.1	0.00	1
16 30 46.2.....	+36 13 07	1.256	15.2	543.3	434.4	0.25	1
16 33 02.2.....	+39 24 27	1.023	17.3	69.6	69.6	0.00	1
16 36 36.4.....	+26 48 09	0.561	40.1	1337.9 ^F	1337.9	0.00	1
17 03 07.7.....	+37 51 25	2.450	19.1	111.1	111.1	0.00	1
17 06 48.1.....	+32 14 22	1.070	53.0	136.2	99.9	0.36	4
21 35 13.1.....	-00 52 43	2.660	58.4	324.4 ^F	323.1	0.00	4
22 14 10.0.....	+00 52 28	0.910	39.6	121.9 ^F	91.8	0.33	1
23 36 24.1.....	+00 02 46	1.100	59.8	227.1 ^F	209.4	0.08	4
23 44 40.0.....	-00 32 31	0.500	168.0	36.4 ^F	18.0	1.02	4
23 47 24.5.....	+00 52 44	0.400	19.1	94.8 ^F	94.8	0.00	2

NOTE.—Data for our sample of 103 FR-II quasars found within the currently available region of the FIRST survey. Units of right ascension are hours, minutes, and seconds, and units of declination are degrees, arcminutes, and arcseconds. The peak-to-peak angular sizes, θ , are measured directly from the FIRST data. The total 1.4 GHz flux densities, S_1 , are taken from the NVSS survey, with a superscripted F indicating that only FIRST fluxes were available for that source. The lobe flux densities, S_l , are obtained by subtracting the FIRST flux of the core component (if any) from S_1 . The core-to-lobe flux density ratio is given by R .

REFERENCES.—The coordinates and redshifts of the quasars are taken from the (1) Veron-Cetty & Veron 1996, (2) Hewitt & Burbidge 1993, and FIRST Bright QSO Survey—(3) Gregg et al. 1996 and (4) R. H. Becker et al. 1997, private communication—catalogs, respectively.

$(1+z)^{-3/2}$ (which corresponds to equal time per bin in an Einstein–de Sitter universe) and with roughly equal numbers per bin, and calculate both the mean values, $\langle\theta\rangle$, and median values, θ_{med} , together with the standard errors of the mean values, and median absolute deviations,¹⁰ respectively, for each bin. The results are shown in Figures 3a–3d, along with the curves from Figure 1, whose amplitudes (corresponding to the mean or median intrinsic sizes) have been scaled to provide a rough visual fit. Before turning to a formal discussion of the results, we describe several important features of the data and address in detail the aforementioned issues associated with properly defining and analyzing such a sample.

1. The most striking feature of the data is that, regardless of the binning details, the observed data seem to be more consistent with Friedmann models than with a Euclidean model. The Friedmann curves shown are not the best-fit results but are merely intended for qualitative reference. We defer the discussion of the best-fit values (§ 4) until after we have addressed the properties and analysis of the sample, including potential problems. It can immediately be seen, however, that while the data are generally consistent with curvature models, it is unlikely, given the uncertainties, that the current sample can distinguish with high significance between the different models. Note that in each case, the data point of the first bin appears anomalously high.

2. Since the radio data are derived entirely from one consistent data set (with a single flux limit, beamwidth, and frequency), our sample does not suffer from the potential problems, described in § 1, associated with the mixing of different samples.

3. As expected, we find that for cases where the FIRST and NVSS flux measurements agree, the second moments derived from both survey maps generally agree to within the second moment errors (provided that the source was larger about $\frac{1}{3}$ the NVSS beam, so that structure could be resolved); for cases where the source registered little or no core flux and comparable lobe fluxes, the measured second moments agreed well with the peak-to-peak sizes listed in Table 1. However, in cases where an appreciable core flux is detected and/or the lobe-to-lobe flux ratio differs substantially from unity, the second moments tend to be systematically smaller than the peak-to-peak sizes, confirming that the peak-to-peak distance is indeed a more robust measure of size—using the second moments would have the undesirable effect of introducing or strengthening a

¹⁰ The median is the value about which the sum of the absolute deviations is minimized, just as the mean defines the value about which the rms deviation is minimized.

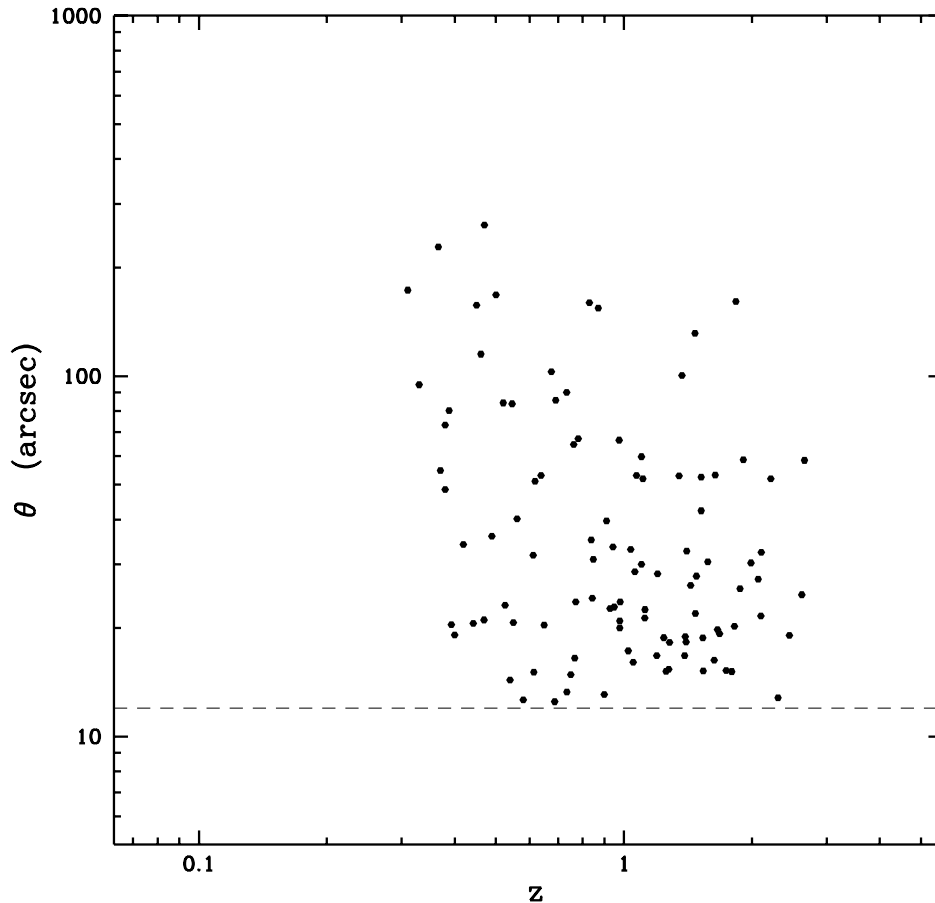


FIG. 2.—Scatter plot of the peak-to-peak angular sizes, θ , vs. redshift. The dashed line represents the effective resolution limit at $12''$, below which accurate morphological classifications could not be determined.

power-size anti-correlation in the data. For sources larger than $\sim 20''$, the measured peak-to-peak sizes agreed closely with those obtained using the model Gaussian fits, as expected.

4. In any flux-limited survey there is the possibility that large, low surface brightness objects could be resolved out. The FIRST survey is sensitive to structure out to $\approx 100''$, and it may be asked whether larger double-lobed sources, whose lobes might equal or exceed this angular size, might be missing from our sample. Since the hot spots of FR-II objects are, by definition, high surface brightness features, and the FIRST survey measures peak fluxes down to ~ 1 mJy, it is highly unlikely that these sources would be missed altogether; only very large, low surface brightness objects can remain undetected, and such sources would not correspond to FR-IIs in our chosen redshift range. If such objects did exist, they would presumably, because of their large sizes and integrated fluxes, be known radio quasars detected by previous surveys and should certainly be detected by the NVSS survey. Thus, to explore this issue in a complete fashion, we individually compared the NVSS and FIRST radio maps for every previously known radio-active quasar in the Veron-Cetty & Veron (1996) catalog falling within the FIRST survey, searching for double-lobed radio sources with sizes up to $1000''$ that might have been missed by FIRST. As expected, we find not a single instance of a large, double-lobed quasar, with $z > 0.3$, detected by NVSS and not by FIRST, indicating that there is no instrumental cutoff at the upper end of the observed angular sizes in our sample. This is confirmed by the fact that, within our chosen redshift range, the upper limit of our θ - z data agrees closely with that of other samples drawn from less sensitive surveys, such as the Third and Fourth Cambridge Catalogs (Hooley et al. 1978; Nilsson et al. 1993).

5. To confirm that our selected sample is not contaminated by FR-I sources, we calculate the intrinsic 1.4 GHz power,

$$P = 4\pi S_{1.4} D_A^2 (1+z)^{3+\alpha}, \quad (2)$$

of each double-lobed quasar, where $S_{1.4}$ is the 1.4 GHz flux density and α is the radio spectral index ($S_\nu \propto \nu^{-\alpha}$). We assume standard values of $\alpha = 0.5$ for any core components, $\alpha = 0.8$ for lobe components (e.g., Gopal-Krishna & Kulkarni 1992; Rector, Stocke, & Ellingson 1995), and take P to be the total core + lobe power. For $h_0 = 0.5$ and $\Omega_0 = 1.0$, we find a lower limit of $P = 1.45 \times 10^{25} \text{ W Hz}^{-1}$ for our sample, near the observed break which separates FR-IIs from the lower-power FR-Is for this choice of cosmological parameters (Fanaroff & Riley 1974, Neeser et al. 1995; Rector, Stocke, & Ellingson 1995). All but nine sources have intrinsic powers in the range $10^{26} \text{ W Hz}^{-1} < P < 10^{29} \text{ W Hz}^{-1}$, indicating that our sample is indeed composed of FR-IIs.

6. Another advantage of the flux sensitivity of the FIRST survey is that our sample includes sources out to a redshift of 2.7, significantly higher than the redshifts at which the minima in the θ - z curves typically occur for different Friedmann models.

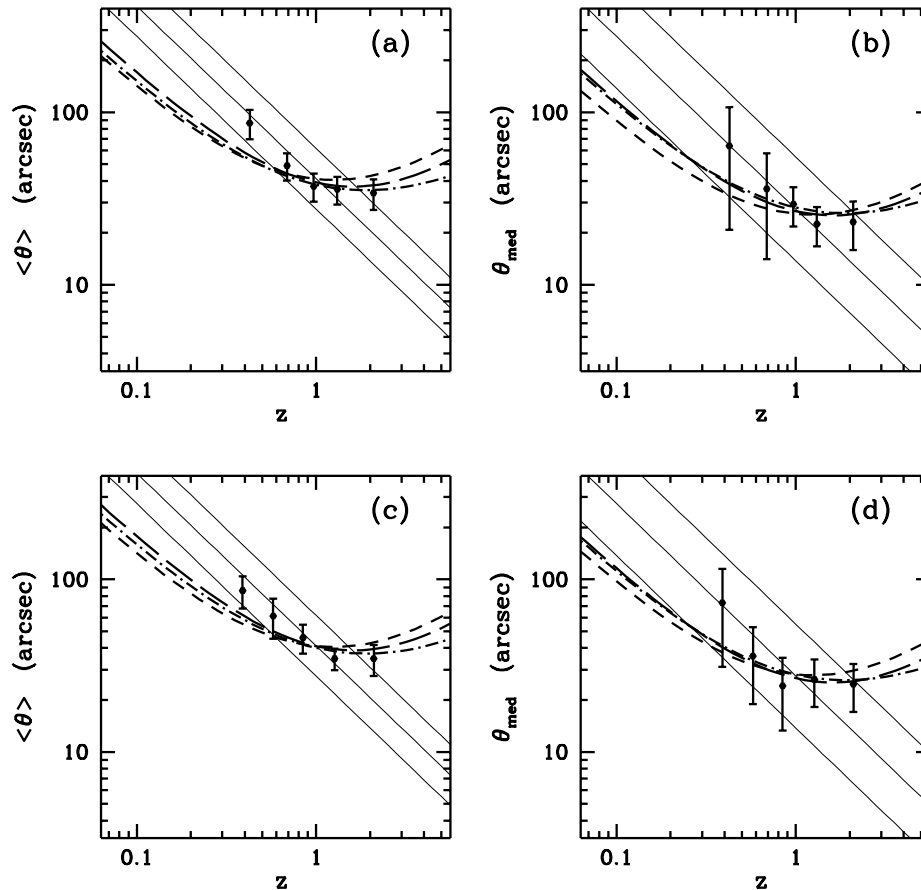


FIG. 3.—Central values of θ vs. redshift using different analytical techniques. In all plots, the short-dashed, long-dashed, and dot-dashed curves are the respective predictions of Friedmann models 1, 2, and 3, assuming the density parameter values listed in Fig. 1, and the thin, solid lines represent Euclidean curves ($\theta \propto z^{-1}$). The curves shown are not the best-fit results but merely visual estimates intended to provide a template for comparison. Note that in all cases, the observed data are generally consistent with curvature and not with Euclidean models. (a) Mean angular size $\langle\theta\rangle$, binned in redshift with roughly equal numbers per bin. The error bars represent the standard errors in the mean values. (b) Median angular sizes, θ_{med} , binned in redshift with roughly equal numbers per bin. The error bars represent the median absolute deviation in each bin. (c) $\langle\theta\rangle$ binned in equal intervals of $(1+z)^{-3/2}$, which corresponds to equal time per bin in an Einstein-de Sitter universe. The error bars represent the standard errors in the mean values. (d) θ_{med} binned in equal intervals of $(1+z)^{-3/2}$. The error bars represent the median absolute deviation in each bin.

This is in contrast to some previous work, which used samples containing significant numbers of sources only to $z \lesssim 1$ (Oort et al. 1987; Kapahi 1989), where roughly Euclidean behavior is expected (see Fig. 1).

7. Like all previous such samples, ours is a subset of the double-lobed radio sources that have measured redshifts and may suffer from the associated selection effects described in § 1. To examine this possibility, we performed a Kolmogorov-Smirnoff (K-S) test to compare the sizes of the double-lobed objects in our sample with those in the FIRST survey as a whole. However, since θ and z are obviously correlated in our sample, with an expected upper limit to the correlation, and we lack complete redshift information for sources in the FIRST survey, we must restrict the test to the range in θ ($\theta < 60''$) below which sources in our sample appear roughly uniformly at every redshift, in order to perform a fair comparison. In the range $12'' < \theta < 60''$ (the origin of the lower limit is discussed below) there are currently 13,664 objects in the FIRST survey that are classified as true double-lobed sources at the 95% confidence level, based on morphology, positional and flux information (Buchalter et al. 1998), and two-point correlation analysis (Cress et al. 1996). A K-S test shows that the null hypothesis—that our size-restricted subsample is drawn from this larger set—can only be rejected only at the 51% level; i.e., it fails to discriminate between the two distributions at the 1σ level. In addition, since 47% of the extended ($> 2''$) sources in the FIRST survey have measured fluxes below 3 mJy, but only five of our 103 sources have either lobe flux in this range, we further restrict the K-S test to sources whose individual lobe fluxes are greater than 3 mJy. In this case we find that the null hypothesis that our remaining subsample is drawn from the 10,521 such sources in the survey can only be rejected only at the 30% level. Furthermore, it is estimated that the median redshift of the FIRST survey is ~ 1.0 (Cress & Kamionkowski 1997), while the median redshift of our sample is 0.98. This evidence, taken together, indicates that the two populations have similar distributions, and therefore that our optically selected sample (i.e., FR-II quasars with measured redshifts) is fairly representative of double-lobed radio sources as a whole. This suggests that no serious selection effects arise from measuring the radio sizes of a largely optically selected subset of double-lobed quasars.

8. Since our sample excludes objects classified as radio galaxies, we avoid the possibility that different mean orientations between quasars and radio galaxies, in the context of the unified scheme, can be introducing noncosmological effects into the θ - z plane. However, the FR-II quasars in our sample do span a range of core-to-lobe flux density ratios, R , suggesting that

they are composed of both CDQs and LDQs. If the redshift distributions of these two populations are different, such effects may still arise. For example, if the fraction of CDQs increases with redshift then the angular sizes of our sources at higher redshifts would be depressed relative to the cosmological predictions, since the CDQs are projected more closely to the line of sight. To investigate this issue, we perform a K-S test to compare the redshift distributions of these two classes of quasars in our sample. Since the observed median values of R for these objects are $R_{\text{CDQ}} \sim 10$ and $R_{\text{LDQ}} \sim 0.1$ (Ubachukwu 1996), we classify our sources using the geometric mean of $R = 1$ for the critical value. This yields 12 CDQs and 91 LDQs in our sample, whose redshift distributions can be distinguished at only the 2% confidence level; i.e., the probability that they are drawn from the same distribution is 98%. Since many of the objects in our sample do not register a core component in the FIRST survey, we also perform a K-S test using a critical value of $R = 0.1$, which divides the sample more evenly into 47 “CDQs” and 56 “LDQs.” In this case, the null hypothesis that the two redshift distributions are drawn from different populations can only be rejected at the 38% level (i.e., they cannot be distinguished at the 1σ level). Since CDQs and LDQs in our sample do not exhibit significantly different redshift distributions, the expected differences in their mean orientations should not alter the θ - z results. More specifically, since

$$R = \frac{R_T}{2} [(1 + \beta \cos \phi)^{-2} + (1 - \beta \cos \phi)^{-2}] \quad (3)$$

(Ubachukwu 1996), where R_T is the value of R when $\phi = 90^\circ$ and $\beta = v/c$ is the flow speed in units of the speed of light (related to the Lorentz factor), the apparent lack of a correlation between R and z suggests that ϕ and z are uncorrelated, and thus that we are looking at a similar distribution of projection angles at every redshift.

9. With a $5''.4$ FWHM beam, the FIRST survey can detect extended structure down to $2''$ (White et al. 1997). However, due to the survey resolution limit, uncertainties in the quasar optical positions, and variations in the morphologies of double-lobed objects, sources with $\theta \lesssim 10''$ could not be assigned an accurate morphological classification. Thus, based on inspection of numerous FIRST radio maps, we have introduced an effective cutoff in the data at $12''$, illustrated by the thin dashed line in Figure 2. In terms of defining a population of standard rods, it is, in fact, *desirable* to have such a cutoff, in order to eliminate the possibility of including so-called core-jet, diffuse, cometary, and other types of extended radio sources that may be mistaken for double-lobed objects at low resolution (cf. § 1). We now outline a self-consistent method for incorporating this cutoff into the analysis.

2.3. Optimizing the Analysis

Consider the parameter space defined by the comoving intrinsic sizes, l , and projection angles, ϕ , of FR-II quasars, as illustrated in Figure 4. In general, the intrinsic sizes will range up to some maximum value, l_{max} , defined by the upper envelope to the observed angular sizes, and above which there simply are no objects (see Fig. 2). Determining the exact value of l_{max} from a given θ - z data set would require assumptions about the cosmology (see eq. [1]), but the actual value is irrelevant for the purposes of this discussion and no such assumptions need be made. The projection angles will range between 0 and some upper limit ϕ_u , which for a randomly distributed population would correspond to 90° , but in the context of the unified scheme would correspond to a value of roughly 45° (Barthel 1989; Lister et al. 1994). The accessible portion of the parameter space is then defined by the largest heavy rectangle in Figure 4. There will also in general be some probability density along each axis, given by $P(l)$ and $P(\phi)$ (assumed to be independent), which will determine the forms of the distributions. For a distribution of randomly oriented rods, it can be seen from simple geometric arguments that $P(\phi) = \sin \phi$ (Harwit 1988, p. 111); $P(l)$ is still a matter of theoretical and observational debate.

Since we are interested in defining a uniform population of objects with true double-lobed structure, it makes sense to impose an effective resolution cutoff at the angular scale for which morphologies are well determined. However, since a constant minimum resolvable angular size does not translate into a constant minimum intrinsic linear size, the effect of this cutoff (or simply of the survey resolution limit in general) will be to introduce a redshift dependence to the intrinsic size distribution. It is desirable therefore to impose a minimum intrinsic size, l_{min} , such that, for a given survey resolution, restricting a sample to sizes $l > l_{\text{min}}$ both avoids potential contamination by misclassified sources *and* preserves the same range of observed sizes at every redshift. It may be expected that the average size of this more homogeneous population (true double-lobed objects with $l_{\text{min}} < l < l_{\text{max}}$) is a more suitable measure of a standard rod than that of a distribution which includes objects with structure down to the resolution limits of various surveys, probing different intrinsic length scales, and possibly mixing different classes of sources.

Since the θ - z relation always exhibits a minimum in Friedmann models, when fitting a given cosmological model to the data, one can define a subsample in which all objects have $l > l_{\text{min}}$ by aligning the minimum of the θ - z curve for that particular model with the smallest observable *angular* size at which morphologies can be accurately determined and including only points above this curve. The choice of l_{min} is, then, determined by whatever value achieves this alignment for the given model, though the actual value is immaterial. The value of l_{max} can be determined by finding the highest amplitude θ - z curve for the given model that still passes through a data point in the sample and thus defines an upper envelope to the angular sizes. The sample so defined will include maximally deprojected objects of intrinsic size l_{min} , and larger objects viewed down to some projection angle given by the heavy, dot-dashed curve in Figure 4 (for example, objects with size l_{max} can be seen projected down to an angle of ϕ'). For the purposes of this analysis, however, one is free to examine only those sources with $l_{\text{min}} < l < l_u$, where l_u can assume any value between l_{min} and l_{max} ; i.e., the discussion presented here is valid for any choice of an upper envelope to the data that is lower than the θ - z curve corresponding to l_{max} and above that corresponding to l_{min} , for the assumed model. For an arbitrary choice of l_u , which we denote by l_* , the sample will include maximally deprojected objects of intrinsic size l_{min} , objects with $l_{\text{min}} < l < l_*$ viewed from ϕ_u down to some projection angle given by the heavy, dot-dashed

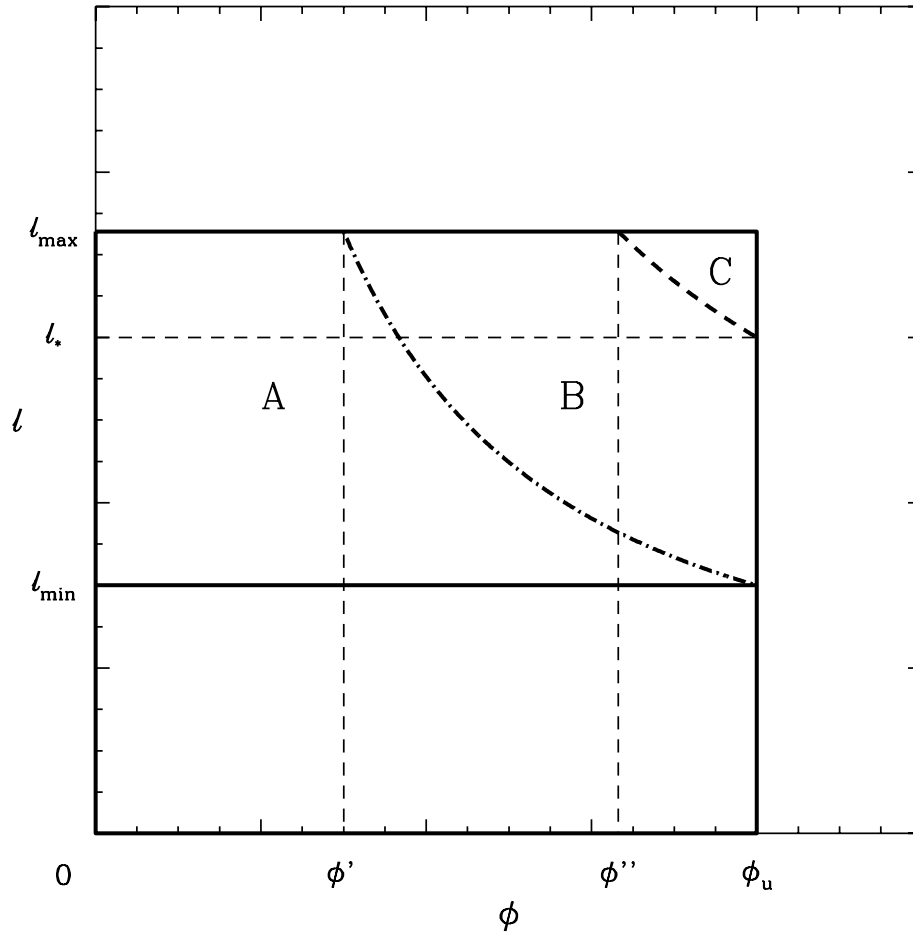


FIG. 4.—The parameter space defined by the intrinsic sizes, l (ordinate), and projection angles with respect to the line of sight, ϕ (abscissa), of FR-II quasars. The values of l can range from 0 to an arbitrary l_{\max} , while ϕ ranges from 0 to some upper limit, ϕ_u , which would correspond to 90° for randomly oriented quasars, or $\sim 45^\circ$ according to unification models, so that the largest heavy rectangle represents the accessible portion of the space. For a survey with a given resolution limit, we define an intrinsic size, l_{\min} , so that maximally deprojected sources with this size correspond to the smallest angular scale at which morphologies can be accurately determined. Any objects intrinsically larger than l_{\min} can then be accurately classified if their projection angles exceed some critical value, given by the dot-dashed line (e.g., objects with $l = l_{\max}$ can be accurately classified with ϕ ranging down to ϕ'). Thus, the combined areas of regions B and C define the subspace of an accurately classified sample of sources with $l_{\min} < l < l_{\max}$ from a single radio survey. In general, one can introduce an upper limit $l_u = l_* < l_{\max}$, which will exclude objects larger than l_* if their projection angles lie to the right of the heavy, dashed line, thus limiting the sample to region B .

curve, and objects with $l_* < l < l_{\max}$ with projection angles between the dashed and dot-dashed heavy curves. The objects in the sample will thus be located either in the combined area of regions B and C (hereafter denoted by BC) in Figure 4 (for an upper envelope corresponding to $l_u = l_{\max}$), or simply in region B (for an upper envelope corresponding to $l_u = l_* < l_{\max}$), and the observed angular sizes, θ , for a given Friedmann model correspond to the distribution of $(l \sin \phi)/D_A$ in these regions. Because of projection effects, some fraction of the objects with intrinsic sizes larger than l_{\min} will be missed (corresponding to region A the figure). If $P(l)$ and $P(\phi)$ were known, it would be a simple matter to calculate the fraction of objects in region A , as well as the $l \sin \phi$ distribution in this region. However, if $P(l)$ and $P(\phi)$ are independent of redshift, then for a given data set, the best-fit values of Ω_0 and Ω_Λ for a particular model can be uniquely determined by the observed θ distribution in any given region and are independent of $P(l)$, $P(\phi)$, and the intrinsic size limits given by l_{\min} , l_{\max} , and ϕ_u . In other words, as long as the distribution of intrinsic projected sizes, $l \sin \phi$, is not sensitive to redshift, the actual values of l_{\min} , l_{\max} , and ϕ_u can only change the amplitude of the best-fit curve to the θ - z data (cf. eq. [1]), not its shape. In contrast, a determination of H_0 would require specific assumptions about these quantities and about $P(l)$. Moreover, even if the $l \sin \phi$ distribution does vary with redshift (e.g., because of some combination of size evolution, a power-size correlation, or orientation effects), Ω_0 and Ω_Λ can still be determined to the extent that this variation can be modeled and corrected for in the data.

The question of whether or not $l \sin \phi$ is independent of redshift is addressed quantitatively in the following section. Note, however, that Figure 3 effectively demonstrates that any relation between $l \sin \phi$ and z cannot be strong; these graphs include all the observed data, without incorporating any of the above size considerations, and are already seen to be fairly consistent with the conventional curvature models, without invoking any redshift evolution of the apparent sizes. We will hereafter use the term “intrinsic size evolution” to denote the case where the intrinsic projected sizes, $s = l \sin \phi$, have a direct correlation with redshift [e.g., if $l \propto (1 + z)^n$ with $n \neq 0$, or if ϕ and z are directly correlated] and “apparent size evolution” to denote the case where s and z are directly and/or indirectly correlated. Thus, apparent size evolution can arise from intrinsic size evolution but also from other effects, such as an l - P correlation coupled with a P - z correlation. In general, various possible

correlations may exist between l , ϕ , P , and z , and we investigate these in detail in § 3. However, only those that give rise to apparent size evolution—an observed correlation between s and z —can affect the determination of cosmological parameters from a given data set.

In the scenario we have presented, the best-fit cosmological parameters to a given data set can be found by exploring parameter space in the following fashion: (1) Assume a particular cosmological model (we use the word “model” as in § 1 to refer to the overall geometry and not the particular values chosen for Ω_0 and Ω_Λ). (2) Adopt trial values for the relevant density parameters in that model. (3) Find the θ - z curve arising from these values (as in Fig. 1), and align the minimum value of this curve with the constant value of the effective angular size cutoff determined for the survey in question. Denote this curve by $\theta_l(z)$. This then fixes the minimum intrinsic size for which accurately determined morphologies in the sample are assured. In a similar manner, adjust the amplitude of the trial θ - z curve so that it lies at some desired level above $\theta_l(z)$, and denote this curve by $\theta_u(z)$. For example, to include all the data above $\theta_l(z)$, one would choose $\theta_u(z)$ so that it defines the upper envelope to the observed angular sizes (corresponding to $l_u = l_{\max}$). (4) Beginning with all the data above the effective cutoff, eliminate any data in the θ - z plane with $\theta < \theta_l(z)$ or $\theta > \theta_u(z)$, thus ensuring that the remaining sources all have intrinsic sizes between l_{\min} and l_u . This step assures that the intrinsic size limits have been imposed in a self-consistent manner. (5) Using the remaining data, perform a χ^2 goodness-of-fit test to determine the best-fit values of the remaining free parameters in the test model (e.g., amplitude and size evolution parameter), and assess how well the output parameters for the assumed model fit the resulting θ - z data. The entire procedure can then be repeated so as to span the range of density parameters appropriate to the assumed model, as well as to explore different models. Conducting the analysis in this fashion both defines a sample whose mean size is more akin to a standard rod and accounts for the limited survey resolution in a self-consistent manner.

3. CORRELATIONS BETWEEN POWER, SIZE, AND REDSHIFT

3.1. Parametric Analysis

Correlations among the properties of FR-II quasars have important implications for understanding the characteristics of the host active galactic nuclei and the evolution of the intergalactic medium, as well as for determining the best-fit cosmological parameters from classical cosmological tests such as the θ - z relation. These correlations must be considered in detail if these objects are to be used as probes of the geometry of the universe. Thus, before addressing cosmological issues, we explore the relationships between the intrinsic properties of the sources in our sample, by spanning the entire assumed range of cosmological parameter values and testing for correlations among the intrinsic properties in each case. For a given set of cosmological parameters, one can calculate respectively the intrinsic power and projected linear size,

$$P = 4\pi S_{1.4} D_A^2 (1+z)^{3+\alpha}, \quad s = l \sin \phi = \theta D_A, \quad (4)$$

of each double-lobed quasar, where we again assume a spectral index of $\alpha = 0.5$ for any core components, $\alpha = 0.8$ for lobe components, and take P to be the total core + lobe power.

If we assume relationships between P , l , and z of the form

$$l \propto (1+z)^n, \quad (5)$$

$$P \propto (1+z)^x, \quad (6)$$

$$l \propto P^\beta, \quad (7)$$

as in § 1, we can then determine the best-fit values of n , x , and β . In practice, it is straightforward to fit for the P - z and l - P correlations, since these are expected to operate independently of the third variable; a P - z correlation should arise from the flux-limited nature of the survey, and an l - P correlation should operate over the lifetime of the sources, which is far less than the cosmological timescales spanned by the z -distribution. Any observed l - z correlation, however, may be due to the separate correlations of l and z with P and not to intrinsic size evolution. To address this possibility, previous authors have investigated the l - z correlation for sources within relatively narrow ranges of intrinsic power, so as to minimize the effect of any dependence on P (Hooley et al. 1978; Kapahi 1985; Singal 1988, 1993; Barthel & Miley 1988; Nilsson et al. 1993). However, according to relations (5)–(7), the combined effects of intrinsic size evolution and a power-size correlation will result in an overall apparent l - z correlation of the form $\theta \propto l \propto (1+z)^c$, where $c = \beta x + n$. Thus, the value of c for a given model follows directly from the data, and, together with the derived values of β and x , one can arrive at a value for n .

We explore models 1 ($\Omega_0 \equiv 1$), 2, and 3, adopting values of Ω_0 from 0.01 to 0.99 inclusive, in intervals of 0.01, for models 2 and 3 (h_0 merely fixes the constants of proportionality in relations [5]–[7] and has no effect on β , x , or n , and all three models obviously yield the same results for $\Omega_0 = 1$), for a total of 199 possible scenarios. For each scenario, we align the corresponding θ - z curve with the effective cutoff at $12''$ and include only data above this curve [denoted by $\theta_l(z)$] and below some upper curve [denoted by $\theta_u(z)$], which may correspond to the true upper envelope to the data, but we can in general assume any lower amplitude still above that of $\theta_l(z)$, as outlined above. For the remaining data, we compute, using five roughly equally populated bins, the mean intrinsic projected sizes, $\langle s \rangle$, in bins of P , $\langle s \rangle$ in bins of z , and $\langle P \rangle$ in bins of z , together with the standard errors in these quantities, and use a χ^2 minimization routine to determine β , c , and x , respectively. We bin the data since we do not have a priori knowledge, independent of cosmological parameter values, of the inherent scatters associated with the various intrinsic properties of these sources and by which the χ^2 values must be weighted; a binned analysis allows us to obtain unbiased estimates for these scatters in each bin. Note that while the intrinsic sizes l appear in relations (5) and (7), we can obtain only the intrinsic *projected* sizes, $s = l \sin \phi$. Using the mean values, $\langle l \sin \phi \rangle$, in each bin properly accounts for the presence of projection effects only if the objects in each bin have similar distributions of ϕ . Otherwise, the derived values of β , c , and n could reflect variations of P and z with respect to ϕ as well as l , and some explicit ϕ dependence would

need to be added to relations (5)–(7) to break this degeneracy. Since we cannot directly test for ϕ correlations parametrically without knowledge of the distributions of R_T and v/c in equation (3), we explicitly use $\langle s \rangle$ rather than $\langle l \rangle$, with the understanding that these are interchangeable only if the ϕ distributions are consistent in each bin. However, we have already concluded, from the K-S tests of the R values in different redshift bins (§ 2.2), that ϕ does not vary significantly with redshift; we discuss further the ϕ distribution below.

The derived values of c , β , and x , as well as the inferred values of n , together with the 1σ errors in each quantity, are listed in the fourth through seventh columns in the top half of Table 2 for a representative seven of the 199 scenarios. These results are obtained using all the data above $\theta_l(z)$ (i.e., ranging to the upper envelope defined by some value $l_u = l_{\max}$) and are thus denoted by an upper limit of l_{\max} in the table. All 1σ errors quoted in this section correspond to the square roots of the appropriate diagonal elements of the covariance matrix for that χ^2 fit (i.e., they are the errors obtained with Ω_0 fixed at its trial value and the corresponding constant of proportionality from relations [5]–[7] fixed at its best-fit value). For all scenarios, we find a strong ($\geq 10 \sigma$) correlation between $\langle P \rangle$ and z , which is expected because of the flux-limited nature of the survey. We also find an inverse correlation, at the 2 – 3σ level between $\langle s \rangle$ and P , which can be understood in terms of the gradual fading of these sources as the lobes expand over timescales ($\sim 10^8$ yr) much shorter than D_A/c , which is indeed the case for quasars in our sample. Previous studies have found $\beta \approx 0.3 \pm 0.1$ for double-lobed quasars assuming an Einstein–de Sitter universe (Oort et al. 1987; Kapahi 1989; Gopal-Krishna & Kulkarni 1992; Chyży & Zięba 1993; Nilsson et al. 1993; Singal 1993), which is consistent with our result for model 1. Table 2 also shows that the observed data ranging up to l_{\max} exhibit mild apparent size evolution at the $\sim 2 \sigma$ level, with all scenarios yielding $c \approx -0.8 \pm 0.4$. Interestingly, however, the data imply little or no intrinsic size evolution; all cases yield a slightly negative $\langle s \rangle$ - z correlation with $-0.4 < n < 0.0$ but are consistent with $n = 0$ well within the 1σ level. The anticorrelation between intrinsic projected size and redshift (given by c) seems to arise mainly from the separate correlations of these quantities with intrinsic power. The lack of intrinsic size evolution in double-lobed quasar samples has been seen by other authors as well (Masson 1980; Singal 1993; Nilsson et al. 1993).

There is also the possibility that the $\langle l \sin \phi \rangle$ - P anticorrelation arises not from intrinsically smaller objects having larger lobe powers but rather from objects projected close to the line of sight (CDQs) having relativistically boosted core power contributing significantly to the total power. In other words, the correlation could arise from different ϕ distributions in different power bins rather than a true power-size correlation. To explore this possibility, we re-solve for β , x , and n using only the lobe power, P_l , which, unlike the total power, is not expected to vary with ϕ . The resulting quantities, denoted by β_l , x_l , and n_l (c remains unchanged) are listed in the eight through tenth columns in the top half of Table 2. Though differing slightly, the values of β_l are all within 1σ of the corresponding values for β and still yield an inverse correlation between $\langle s \rangle$ and P_l , at the 2 – 3σ level in all cases, indicating that, while orientation effects may be present, they are not primarily responsible for producing the observed anticorrelation between intrinsic projected size and power. Similarly, the values for n_l differ slightly from those of n , in some cases having a different sign, but still agree to well within the 1σ level, implying that the $\langle l \sin \phi \rangle$ - z correlation does not arise primarily from a ϕ - z correlation. As expected, the values of x_l are not significantly different from x , since cosmological surface brightness dimming affects P and P_l in a similar fashion.

We have shown that the $\langle l \sin \phi \rangle$ - P correlation is not the result of orientation effects but rather is due to a negative correlation between l and P and, furthermore, that this correlation, coupled with the P - z relationship, appears largely to account for the apparent size evolution in the data. Inspection of various scatter plots of the data for the different scenarios supports these conclusions, suggesting that the negative $\langle s \rangle$ - P correlation arises mainly from the fact that the ~ 20 largest projected sources in the sample have low values of P and lie preferentially at lower redshifts. We have already seen, however, that one need not choose the amplitude of $\theta_u(z)$ to trace the upper envelope to the θ - z data (i.e., to l_{\max}), but one can, in principle, choose any value between this and $\theta_l(z)$ without loss of generality or the introduction of sample bias. Thus, in light of the above conclusions, we rederive the values of c , β , x , and n , fixing the $\theta_u(z)$ curve in each scenario to have a minimum at $65''$ (corresponding to some intrinsic size $l_u = l_*$), which eliminates roughly 20 of the largest sources in each scenario. The

TABLE 2
SELECTED RESULTS OF PARAMETRIC FITS FOR c , β , x , AND n

Model	Ω_0	Limit	c	β	x	n	β_l	x_l	n_l
1.....	1.00	l_{\max}	-0.828 ± 0.379	-0.168 ± 0.067	3.672 ± 0.376	-0.211 ± 0.456	-0.150 ± 0.066	3.793 ± 0.404	-0.260 ± 0.457
2.....	0.10	l_{\max}	-0.827 ± 0.423	-0.102 ± 0.061	4.513 ± 0.352	-0.366 ± 0.507	-0.182 ± 0.059	4.644 ± 0.380	0.017 ± 0.509
2.....	0.30	l_{\max}	-0.694 ± 0.362	-0.117 ± 0.061	3.993 ± 0.350	-0.227 ± 0.439	-0.197 ± 0.067	4.094 ± 0.376	0.114 ± 0.459
2.....	0.90	l_{\max}	-0.808 ± 0.378	-0.166 ± 0.067	3.712 ± 0.375	-0.193 ± 0.457	-0.148 ± 0.065	3.835 ± 0.403	-0.242 ± 0.458
3.....	0.10	l_{\max}	-0.853 ± 0.427	-0.121 ± 0.061	4.280 ± 0.364	-0.335 ± 0.502	-0.182 ± 0.062	4.399 ± 0.392	-0.054 ± 0.512
3.....	0.30	l_{\max}	-0.678 ± 0.366	-0.113 ± 0.063	4.087 ± 0.357	-0.217 ± 0.449	-0.167 ± 0.062	4.198 ± 0.382	0.024 ± 0.454
3.....	0.90	l_{\max}	-0.800 ± 0.379	-0.164 ± 0.067	3.725 ± 0.376	-0.187 ± 0.457	-0.147 ± 0.065	3.847 ± 0.404	-0.236 ± 0.458
1.....	1.00	l_*	-0.142 ± 0.225	-0.098 ± 0.044	2.843 ± 0.445	0.137 ± 0.262	-0.090 ± 0.041	2.884 ± 0.496	0.117 ± 0.258
2.....	0.10	l_*	-0.141 ± 0.221	-0.064 ± 0.042	3.462 ± 0.442	0.082 ± 0.266	-0.067 ± 0.039	3.424 ± 0.484	0.090 ± 0.260
2.....	0.30	l_*	-0.108 ± 0.232	-0.062 ± 0.044	3.204 ± 0.433	0.092 ± 0.272	-0.063 ± 0.041	3.231 ± 0.477	0.094 ± 0.268
2.....	0.90	l_*	-0.122 ± 0.225	-0.095 ± 0.044	2.878 ± 0.444	0.152 ± 0.261	-0.088 ± 0.041	2.921 ± 0.495	0.134 ± 0.258
3.....	0.10	l_*	-0.168 ± 0.232	-0.068 ± 0.043	3.332 ± 0.449	0.058 ± 0.274	-0.071 ± 0.039	3.351 ± 0.492	0.070 ± 0.269
3.....	0.30	l_*	-0.153 ± 0.230	-0.065 ± 0.042	3.679 ± 0.389	0.084 ± 0.277	-0.066 ± 0.040	3.650 ± 0.450	0.088 ± 0.273
3.....	0.90	l_*	-0.114 ± 0.225	-0.094 ± 0.044	2.895 ± 0.445	0.159 ± 0.262	-0.087 ± 0.041	2.938 ± 0.496	0.141 ± 0.259

NOTE.—The values for β , x , and n are obtained using the total power, P , while those for β_l , x_l , and n_l are obtained using only the lobe power, P_l . Note that these two sets of values agree to within the 1σ errors listed. A limit of l_{\max} means that all data points above the θ - z curve corresponding to l_{\min} for the given model were used, while a limit of l_* means that points lying above the θ - z curve with a minimum at $65''$ for that choice of Ω_0 were rejected, corresponding to the subsample with $c \approx 0$.

removal of these sources reduces the seemingly anomalously high values in the first redshift bins of Figures 3a–3d and also eliminates the few exceptionally large sources at $z > 1$ (see Fig. 2). The results obtained from the remaining samples for the same seven scenarios are presented in the lower half of Table 2, where they are denoted by an upper limit of l_* . We indeed find that, in all trial cases, the magnitude of the $\langle s \rangle$ - P correlation diminishes significantly, with $-0.11 < \beta < 0.0$ in all cases, and is generally consistent with zero at the $\lesssim 2 \sigma$ level. The $\langle P \rangle$ - z correlation remains highly significant, as expected. The derived values for n become positive, rather than negative, in all cases but are generally much smaller in magnitude than those obtained using an upper limit of l_{\max} and are certainly consistent with $n = 0$ well within the 1σ range. Most important, we find, as expected for the l_* samples, that there is no significant apparent size evolution, with c consistent with zero well within the 1σ level for all scenarios. These results confirm that large, fainter sources (which can be seen only at lower redshifts) were largely responsible for the power-size correlation and resulting apparent size evolution observed previously and suggest that we can define a sample whose θ - z variation should primarily be due to cosmological effects alone. Unlike the case for the samples obtained using an upper limit corresponding to l_{\max} , the values of β_l , x_l , and n_l obtained using l_* , are virtually identical to those for β , x , and n , indicating that for these samples, orientation effects play no role in the $\langle s \rangle$ - z and $\langle s \rangle$ - P correlations.

3.2. Nonparametric Analysis

The analysis of § 3.1 assumes specific functional forms for the relationships between P , l , and z and is valid only insofar as these parameterizations accurately reflect the underlying physics. If this is not the case, the resulting fitted values are merely artifacts of the model, not parameters truly descriptive of the data. For example, the relation $P \propto (1 + z)^x$, though a good approximation, does not properly account for the implicit dependence of D_A on z (see eqs. [1] and [4]). Thus, a better approach to searching for correlations in the data is to employ nonparametric tests that are independent of an assumed functional form. In addition, nonparametric statistics offer another advantage in that they are readily applied to unbinned distributions and thus incorporate information that is lost when the distributions are binned. In particular, the Spearman rank correlation coefficient, r_{ab} , tests, in a nonparametric fashion, the degree to which the quantities a and b are correlated in a given data set, varying from -1 (for strong negative correlation) to $+1$ (for strong positive correlation), with 0 indicating no correlation. The Spearman partial-rank statistic,

$$r_{ab,c} = (r_{ab} - r_{ac}r_{bc}) / \sqrt{(1 - r_{ac}^2)(1 - r_{bc}^2)},$$

has the same range and tests whether there is a significant correlation between a and b that does not arise from both being separately correlated with a third quantity, c ; i.e., it effectively tests for a correlation between a and b if c is held constant. For data sets with ≥ 30 data points, the distribution of $[(n - 1)]^{1/2}r_s$, where r_s is a Spearman statistic, is well approximated by a normal distribution with unit variance (Conover 1980). Thus, for a given data set with an observed Spearman statistic, r_{obs} , one can easily compute the (two sided) probability, p , that a random, uncorrelated data set, with r_{ran} , could exhibit this degree of correlation (positive or negative) or higher (i.e., the probability that $|r_{\text{ran}}| \geq |r_{\text{obs}}|$) and thus obtain the significance of the result. For the correlation coefficient, r_{ab} , this is simply the probability of seeing r_{ab} occur by chance if there is no intrinsic correlation between a and b . For the partial rank statistic, $r_{ab,c}$, it is the probability of seeing $r_{ab,c}$ occur by chance if there is no correlation between a and b other than that caused by their being separately correlated to c .

The upper half of Table 3 shows the results of the rank analysis, listing the Spearman statistics for the various combinations of z , s , and P , and the corresponding values of p (given in parentheses), for the same seven of the 199 trial scenarios from § 3.1 using an upper limit corresponding to l_{\max} . In all cases investigated, we find evidence for a negative correlation between s and z at the 90%–95% confidence level (given by $1 - p$), a significant inverse correlation between s and P , near the 3σ level (i.e., $1 - p > 99\%$), and a highly significant P - z correlation. Moreover, the partial rank correlation coefficient, $r_{sz,P}$ indicates that the s - z correlation arises entirely from the s - P and P - z correlations, so that s and z are intrinsically uncorrelated, with $p > 0.36$ in all cases. Intrinsic size evolution is consistent with zero well within 1σ for all cases and does not account for the mild degree of apparent size evolution. These results all agree closely with our results from the parametric analysis.

TABLE 3
SELECTED RESULTS OF NONPARAMETRIC ANALYSIS BETWEEN s , P , AND z

Model	Ω_0	Limit	r_{sz}	r_{sP}	r_{sPz}	r_{Pz}	$r_{sz,P}$
1	1.00	l_{\max}	-0.196 (0.051)	-0.343 (0.001)	-0.318 (0.002)	0.693 ($< 10^{-11}$)	0.062 (0.536)
2	0.10	l_{\max}	-0.199 (0.057)	-0.329 (0.002)	-0.302 (0.004)	0.749 ($< 10^{-12}$)	0.076 (0.462)
2	0.30	l_{\max}	-0.157 (0.120)	-0.277 (0.006)	-0.258 (0.011)	0.726 ($< 10^{-12}$)	0.067 (0.507)
2	0.90	l_{\max}	-0.188 (0.062)	-0.337 (0.001)	-0.312 (0.002)	0.697 ($< 10^{-11}$)	0.069 (0.488)
3	0.10	l_{\max}	-0.205 (0.048)	-0.314 (0.002)	-0.284 (0.006)	0.746 ($< 10^{-12}$)	0.048 (0.645)
3	0.30	l_{\max}	-0.176 (0.084)	-0.271 (0.008)	-0.243 (0.017)	0.739 ($< 10^{-12}$)	0.036 (0.721)
3	0.90	l_{\max}	-0.183 (0.069)	-0.335 (0.001)	-0.311 (0.002)	0.697 ($< 10^{-11}$)	0.074 (0.458)
1	1.00	l_*	-0.017 (0.874)	-0.211 (0.056)	...	0.634 ($< 10^{-8}$)	...
2	0.10	l_*	-0.059 (0.600)	-0.203 (0.072)	...	0.701 ($< 10^{-9}$)	...
2	0.30	l_*	-0.017 (0.876)	-0.144 (0.186)	...	0.683 ($< 10^{-9}$)	...
2	0.90	l_*	-0.006 (0.957)	-0.200 (0.070)	...	0.637 ($< 10^{-8}$)	...
3	0.10	l_*	-0.073 (0.514)	-0.194 (0.082)	...	0.704 ($< 10^{-9}$)	...
3	0.30	l_*	-0.038 (0.729)	-0.133 (0.228)	...	0.699 ($< 10^{-9}$)	...
3	0.90	l_*	0.001 (0.993)	-0.197 (0.074)	...	0.638 ($< 10^{-8}$)	...

NOTE.—The quantities r_{ab} and $r_{ab,c}$ respectively connote the Spearman rank correlation and partial rank correlation coefficients between quantities a , b , and c . In each case, the number in parenthesis denotes the two-sided probability that a random data set could achieve the associated value of $|r|$ and thus gives the significance of the result.

TABLE 4
SELECTED RESULTS OF NONPARAMETRIC CORRELATIONS WITH R

Model	Ω_0	Limit	r_{Rs}	r_{RP}	r_{RP_c}
1	1.00	l_{\max}	-0.501 ($<10^{-4}$)	-0.052 (0.671)	0.580 ($<10^{-5}$)
2	0.10	l_{\max}	-0.474 ($<10^{-3}$)	-0.006 (0.964)	0.588 ($<10^{-5}$)
2	0.30	l_{\max}	-0.503 ($<10^{-4}$)	-0.046 (0.705)	0.567 ($<10^{-5}$)
2	0.90	l_{\max}	-0.506 ($<10^{-4}$)	-0.053 (0.669)	0.580 ($<10^{-5}$)
3	0.10	l_{\max}	-0.503 ($<10^{-4}$)	-0.038 (0.759)	0.547 ($<10^{-5}$)
3	0.30	l_{\max}	-0.505 ($<10^{-4}$)	-0.042 (0.732)	0.558 ($<10^{-5}$)
3	0.90	l_{\max}	-0.507 ($<10^{-4}$)	-0.053 (0.669)	0.580 ($<10^{-5}$)
1	1.00	l_*	-0.419 (0.003)	-0.125 (0.377)	0.558 ($<10^{-4}$)
2	0.10	l_*	-0.463 (0.001)	0.004 (0.979)	0.631 ($<10^{-5}$)
2	0.30	l_*	-0.484 ($<10^{-3}$)	-0.067 (0.623)	0.581 ($<10^{-4}$)
2	0.90	l_*	-0.427 (0.003)	-0.123 (0.386)	0.562 ($<10^{-4}$)
3	0.10	l_*	-0.506 ($<10^{-3}$)	-0.038 (0.776)	0.573 ($<10^{-4}$)
3	0.30	l_*	-0.486 ($<10^{-3}$)	-0.062 (0.647)	0.571 ($<10^{-4}$)
3	0.90	l_*	-0.428 (0.002)	-0.123 (0.386)	0.562 ($<10^{-4}$)

We also tested s separately against P_l to see whether the s - P correlation was truly due to a power-size correlation (to which P_l is sensitive) and not due to beaming effects (to which P_l is not sensitive). We indeed find that values of r_{sP_l} are close to those for r_{sP} , with the significance level remaining near or above 98% in all cases. We do not directly test for a correlation with P_c , since not all sources registered a FIRST core component, but we do eliminate CDQs, using both criteria of $R > 1.0$ and also $R > 0.5$, re-solve for r_{sz} , and in both cases find similar values to those in Table 3, indicating again that a true power-size correlation, and not beaming effects, are responsible for producing the observed apparent size evolution. Also, since some sources listed as having $P_c = 0$ may in truth have some core flux that was not separately represented in the FIRST catalog, we reperform the analysis including only those sources with $P_c \neq 0$ and again find virtually identical results to those in Table 3.

In the lower half of Table 3 are the results obtained using an upper limit corresponding to $l_u = l_*$ as defined above. Again, we confirm the results of the parametric tests, finding that while the P - z correlation remains highly significant, the s - P correlation is reduced in magnitude, with significance typically below the 2σ level in the various scenarios, and the s - z correlation effectively vanishes in all cases, consistent with zero apparent size evolution. As expected, these results agree with the parametric analysis but are more robust in the sense that they are independent of the assumed model governing the characteristics of the sources.

The nonparametric analysis also allows us to probe the ϕ distributions more directly and examine issues related to unification schemes for radio-loud AGNs. Since R is expected to be correlated with ϕ via equation (3), we can, unlike in the parametric case, test for correlations between some quantity q and ϕ through r_{Rq} without invoking assumptions about the distributions of R_T or v/c . We have already seen that the ϕ distribution is not sensitive to redshift and that it does not account for the observed s - P correlation. However, if the unified scheme is correct, in the sense that sources projected near the line of sight have relativistically boosted core fluxes, then there should be a negative correlation between R and intrinsic projected size, s , and, obviously, a positive correlation between R and the intrinsic core power, P_c , since $R \propto P_c/P_l$. Some sources in the sample may have registered $R = 0$ not because they truly lacked a significant core but, rather, in the case of smaller sources, because the FIRST fitting algorithm did not assign that source a core component. Assigning the flux in such sources to the lobes had no significant effect on the results above, as seen when we omitted sources lacking a measured core component, but could seriously affect apparent correlations with R . Thus we include here only those sources with $R \neq 0$. Table 4 shows the results of the rank tests between various quantities and R for these sources, with the upper and lower sections again corresponding to limits of l_{\max} and l_* , for the same seven of the 199 scenarios. For all cases, we indeed find a significant ($>99.7\%$) inverse correlation between R and s , as predicted by the unified model. Moreover, while R and the total power P show no statistically significant relationship, R and P_c exhibit a positive correlation with high significance ($p < 10^{-4}$) in all cases, as would be expected. Though only suggestive, these results indicate that the behavior of these radio-loud quasars is consistent with the expectations of unification schemes.

4. COSMOLOGICAL PARAMETERS

Having explored the intrinsic properties of the sources over the assumed range of cosmological density parameter values, we now turn to a discussion of the best-fit cosmological results. The cosmological models we consider are models 1, 2, and 3 from § 1, along with a Euclidean model for comparison. Since the results of the nonparametric analysis corroborate those of the parametric analysis, we allow for apparent size evolution in the data of the form $l \propto (1+z)^c$ so that $l \sin \phi = (l \sin \phi)_0(1+z)^c$, where a zero subscript denotes the present-day ($z = 0$) value. To determine the best-fit values for the free parameters in each model, we follow the prescription in § 2.3 and minimize the quantity

$$\chi^2 = \sum_{i=1}^N \left\{ \frac{[\langle \theta_p \rangle(a, c, \Omega_0; z_i) - \theta_i]^2}{\sigma_i^2 + \sigma_\theta^2} \right\}, \quad \langle \theta_p \rangle = \frac{a(1+z)^c}{f(\Omega_0; z)}, \quad (8)$$

where $\langle \theta_p \rangle$ is the mean angular size predicted by the model at z_i , given a , c , and Ω_0 ; the σ_i are the errors associated with the N individual measurements θ_i ; $a = h_0 \langle l \sin \phi \rangle_0$ (measured in Mpc throughout) fixes the overall amplitude of the θ - z curve; and $f(\Omega_0; z) = h_0 D_A$ is given by equation (1). The quantity $\sigma_\theta = \sigma_{l \sin \phi} / D_A$ is the observed root variance in the distribution of θ , which in general arises from the spread in the intrinsic projected sizes, given by $\sigma_{l \sin \phi}$, as well as from curvature effects.

TABLE 5
BEST-FIT PARAMETERS TO THE θ - z DATA

Model	Limit	$\chi^2 (N, \nu, 1 - p)$	a	c	Ω_0
1.....	l_{\max}	1.776 (100, 3, 0.620)	0.32 (0.19, 0.55)	-0.83 (-1.64, -0.12)	1.00
2.....	l_{\max}	0.822 (98, 2, 0.663)	0.35 (0.21, 0.57)	-0.64 (-1.36, -0.12)	0.38 (0.28, 1.00)
3.....	l_{\max}	1.021 (97, 2, 0.600)	0.32 (0.21, 0.50)	-0.61 (-1.37, -0.05)	0.35 (0.25, 1.00)
Euclidean.....	...	6.959 (103, 4, 0.138)	0.57 (0.52, 0.62)
1.....	l_*	0.408 (83, 3, 0.939)	0.15 (0.10, 0.21)	-0.25 (-0.73, -0.29)	1.00
2.....	l_*	0.362 (83, 2, 0.834)	0.15 (0.10, 0.35)	-0.19 (-0.67, -0.31)	0.84 (0.03, 1.00)
3.....	l_*	0.408 (83, 2, 0.816)	0.15 (0.10, 0.29)	-0.23 (-0.66, -0.29)	0.93 (0.00, 1.00)

NOTE.— N denotes the number of points falling within the angular size cutoffs in each case, which is then divided into five bins. For normally distributed data (which ours are not) the value of $1 - p$ would give the significance of the result, where p is the cumulative distribution function for the χ^2 probability function with ν degrees of freedom. Each best-fit parameter value is accompanied by the 1σ confidence limits in parentheses.

Without knowledge of $P(l)$, l_{\min} , l_{\max} , and ϕ_u , we cannot a priori determine $\sigma_{l \sin \phi}$, which fixes the scatter in θ at a given D_A . Therefore, one must resort to a binned analysis to estimate σ_θ from the scatter in θ in different bins. Furthermore, it is clear that the σ_i (typically $\approx 1''$) are much smaller than the scatter in θ at any given redshift and, thus, that $\sigma_i^2 \ll \sigma_\theta^2$, so that we can ignore the σ_i . We thus seek to minimize

$$\chi^2 = \sum_{j=1}^M \left\{ \frac{[\langle \theta_p \rangle(a, c, \Omega_0; z_j) - \langle \theta_j \rangle]^2}{\sigma_{\langle \theta_j \rangle}^2} \right\}, \quad (9)$$

where now the $\langle \theta_p \rangle$ are the predicted mean angular sizes in M bins centered at z_j with observed mean sizes $\langle \theta_j \rangle$ and corresponding standard errors $\sigma_{\langle \theta_j \rangle}$.

Using five roughly equally populated bins, we follow the method outlined in § 2.3 and calculate χ^2 with respect to the free parameters in each model. Model 1, with a fixed value of Ω_0 , has only two free parameters, $a = h_0 \langle l \sin \phi \rangle_0$ (with $a > 0$) and c . The quantity $\langle l \sin \phi \rangle$ appears because it is, by definition, the mean value of θ around which χ^2 will be minimized (cf. eq. [1]). Models 2 and 3 each have three free parameters, a , c , and Ω_0 (with $0 < \Omega_0 \leq 1$). The Euclidean model simply has one free parameter corresponding to the amplitude. For each trial value of Ω_0 in the Friedmann models ($\Omega_0 \equiv 1$ in model 1, and trial values in intervals of 0.01 from 0 to 1 for models 2 and 3), we use the resulting $\theta_l(z)$ and $\theta_u(z)$ curves to ensure a uniform range of intrinsic sizes and then determine the best-fit values of a and c for the remaining data, as well as the value of χ^2 for this set of parameters. In practice, aligning the minimum intrinsic size cutoff of the various Friedmann models with the survey resolution limit, which is vital in terms of producing a self-consistent result, removes three to 17 data points depending on the trial value of Ω_0 , but typically fewer than five for $\Omega_0 > 0.3$. This prescription is meaningless for the Euclidean case, which does not exhibit a minimum in the angular size; for this case we simply follow the approach of past workers and use all the data above the cutoff at $12''$.

The results of our analysis for each of the four models, using $M = 5$ bins containing the various N data points between θ_l and θ_u given by $l_u = l_{\max}$, are shown in the upper part of Table 5, which lists the values of N and χ^2 for each best fit, together with the number of degrees of freedom, ν , in the model, and resulting significance level, $1 - p$, as well as the best-fit values of the free parameters, and the 1σ confidence limits on these values. It should be noted that the values of p are computed under the assumption of normally distributed data. Although the unbinned intrinsic projected sizes, $l \sin \phi$, and thus the angular sizes, θ , given by equation (1), are not expected to follow a normal distribution, or even to be symmetric about their mean values (see Fig. 2), the central limit theorem ensures that, for binned data with a sufficiently large number of points, the distribution of the mean value in each bin (which is, in fact, our dependent variable) will be close to a Gaussian, independent of the underlying distribution. Insofar as we have $\lesssim 20$ points in each bin, the probabilities derived from our χ^2 values might be slightly in error due to any residual non-Gaussianity. Moreover, the lower (and for cases with $l_u = l_*$, upper) tails of the observed θ distribution have been removed by the cuts in our analysis method, thereby enhancing the non-Gaussianity. Thus, while it is straightforward to compute the mean values and calculate the value of χ^2 for each trial model, the formal significance of the result cannot be obtained in a simple, analytic fashion (nor can it be computed numerically without knowing the intrinsic size distribution); the listed values of $1 - p$ for the various models are intended to be qualitatively illustrative of the relative significance levels and not rigorously accurate. Since we have no a priori knowledge of the actual values of the free parameters, all parameter errors quoted here correspond *not* to the diagonal elements of the covariance matrix of the fit (i.e., to the error obtained with the other parameters held fixed at their best-fit values) but rather to the much larger error range subtended by the joint variation in all free parameters, given conservatively by the various one-dimensional projections of the 1σ confidence region in the parameter space. Figure 5 provides a graphical representation of our results.

It is clear that the observed data are entirely consistent with Friedmann models with reasonable values of Ω_0 . The underdense models 2 and 3 both yield $\Omega_0 \approx 0.35$ with a 1σ range including values from ~ 0.25 to 1.00 and exhibit a fairly flat χ^2 surface in this range of parameter space, so that they are truly consistent with the value $\Omega_0 = 1$ required by model 1.¹¹ The constraints implied by model 2 on the energy density associated with the cosmological constant are $\Omega_\Lambda = 0.62$ with 1σ limits ranging from 0 to 0.72. All three Friedmann models are seen to yield roughly equal values of $1 - p$, indicating, as expected,

¹¹ Since Ω_0 in models 2 and 3 was constrained to lie between 0 and 1, the confidence limits explored were similarly restricted to this interval. Fits to closed Friedmann models, with $\langle \theta_p \rangle$ calculated using $\Sigma(x) = \sin x$ in eq. (1), invariably yielded values of χ^2 significantly larger than the minimum value in corresponding nonclosed model. Thus, while values of $\Omega_0 > 1$ in these models did fall within the 1σ range of the best-fit value, we do not consider the results of closed models in the present treatment.

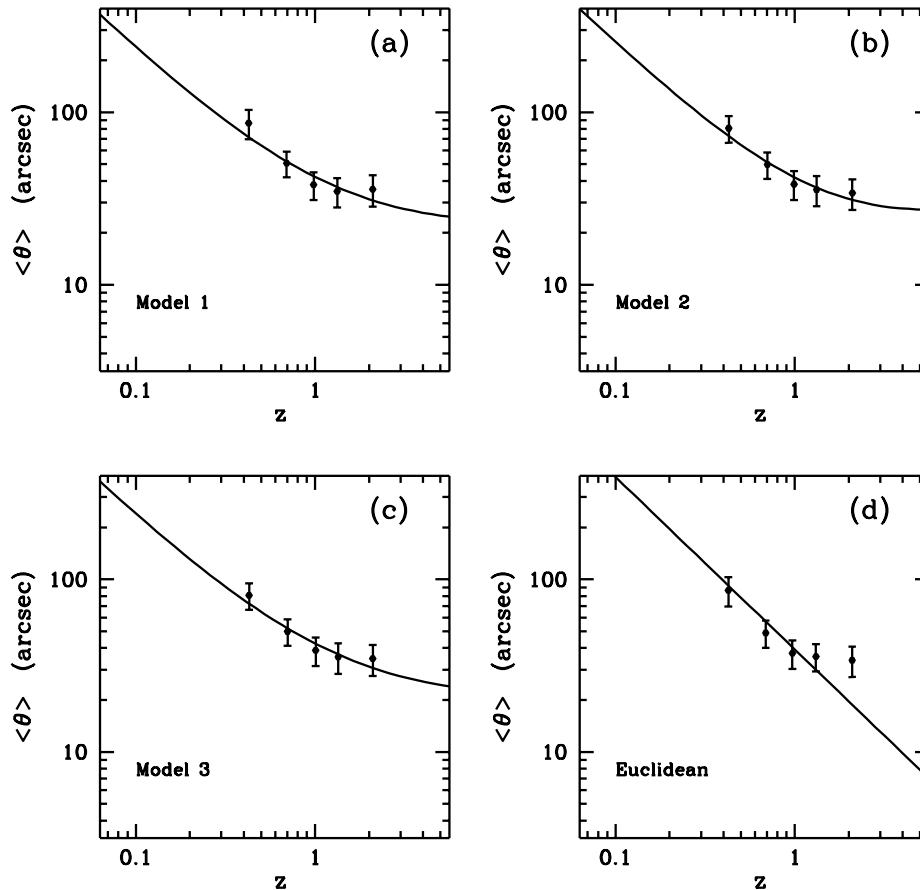


FIG. 5.—Best-fit curves to the θ - z data with $l_u = l_{\max}$ for the various models explored. (a) Model 1 with $a = 0.32$, $c = -0.83$, and $\Omega_0 = 1$. (b) Model 2 with $a = 0.35$, $c = -0.64$, and $\Omega_0 = 0.38$. (c) Model 3 with $a = 0.32$, $c = -0.61$, and $\Omega_0 = 0.35$. (d) Euclidean model with $a = 0.57$. Note that the Friedmann models appear to fit the data equally well, while the Euclidean model constitutes a relatively poor fit.

that the present data cannot effectively discriminate between the various Friedmann models, although interesting constraints on the free parameters within a given model are obtained.¹² It should be pointed out, however, that model 1, which is merely a particular case of models 2 and 3, yields a comparable value of $1 - p$ only because Ω_0 is assumed to be known a priori, thus allowing for an additional degree of freedom in the fit. Any presumed value of Ω_0 within the 1σ range of the best-fit values would similarly yield a fit on par with that of models 2 and 3. To the extent that Ω_0 is not predetermined, there is no particular significance to the results of model 1; it is included primarily because it is the canonical standard among current theoretical models. Note that the best-fit Euclidean model (which uses all the data points) is the only one that yields a reduced χ^2 value, χ^2/ν , greater than unity and is actually a comparatively poor fit to the data. For comparison, we also performed a semi-binned analysis, using the individual values θ_i as in equation (8), rather than the mean of the binned values, but still assign each source a σ_θ corresponding to the standard deviation of the angular sizes in the bin corresponding to that source (i.e., we use the binned values of σ_θ , but not of θ_i), and obtain roughly identical results for the best-fit parameters in each model.

As expected from the results of § 3, the data appear to require mild apparent size evolution with $c \approx -0.8$ for model 1 and $c \approx -0.6$ for both models 2 and 3. We have seen that this trend arises primarily from a power-size correlation, rather than from intrinsic size evolution or orientation effects between CDQs and LDQs (orientation differences between radio galaxies and quasars are ruled out since we have included only the latter in our sample). The values obtained here for c agree closely with the corresponding results from § 3 but differ slightly because we have here assigned each source the value of D_A corresponding to its bin, so that $\langle \theta_j \rangle D_{A_j} \propto (1+z)^c$ over the j bins, rather than taking $\langle \theta_i \rangle D_{A_i}$ for each of the i sources, and then binning the projected sizes, as in § 3. The error ranges also differ since, as described above, we have here taken the errors to arise from the joint variation of all free parameters. An inspection of the variation of χ^2 with respect to the free parameters reveals that χ^2 in a given model is significantly more sensitive to changes in c than in Ω_0 ; i.e., $|d\chi^2/dc| > |d\chi^2/d\Omega_0|$. Therefore, since the effect of $c < 0$ is to decrease the apparent sizes of sources at higher redshifts, mimicking a decrease in Ω_0 , we may infer that, for models 2 and 3, the best-fit values for Ω_0 obtained using an upper limit corresponding to $l_u = l_{\max}$ are likely lower limits to the actual values. We have already seen, however, that we can define a sample for which apparent size evolution is minimal, and for which the derived values of Ω_0 should therefore correspond more closely to the actual values. The lower part of Table 5 shows the results obtained using an upper limit corresponding to $l_u = l_*$. In this case, we see that all models yield $c \approx -0.2 \pm 0.5$ and do indeed find higher best-fit values of 0.84 and 0.93, respectively, for Ω_0 in models 2 and 3, appearing to

¹² Kellerman 1993, looking at the sizes of compact sources on milliarcsecond scales, found the θ - z relation to be consistent with an Einstein-de Sitter universe, but did not consider other possible models; Krauss & Schramm 1993.

favor a flat universe. The lower amplitude of the $\theta_u(z)$ curve, however, removes $\sim 20\%$ of the data, and the resulting sample yields larger errors on Ω_0 in models 2 and 3, effectively spanning the range from 0 to 1. In this case, model 2 yields $\Omega_\Lambda = 0.16$ with 1σ limits of 0.0 and 0.97. We also find that while all three models again fit the data with high significance, that model 1, with $\Omega_0 = 1$, appears to be slightly favored, subject to the qualification discussed above. Since all three models yield similar values for Ω_0 , as well as a and c , in the $l_u = l_*$ case, they each pick out the same 83 data points and are thus all plotted on the same graph in Figure 6, where they are seen to virtually overlap.

In principle, we could test the robustness of the zero apparent size evolution feature of the $l_u = l_*$ data and of our analytic methods by raising the amplitude of the $\theta_l(z)$ curve, effectively mimicking a survey with poorer angular resolution. If apparent size evolution was not truly absent, then performing our analysis with a higher survey cutoff would selectively eliminate different fractions of sources in different redshift bins, changing the value of $\langle l \sin \phi \rangle$ in each bin by different amounts and thus producing a different value for Ω_0 . On the other hand, if the angular size distributions truly are redshift independent, raising the resolution cutoff in our analysis would remove the same fraction of sources in each bin (those with sizes below the new value of l_{\min}), changing the amplitude of the best-fit curve but not its shape. We would thus expect to find a different, higher value for a , but the same value for Ω_0 . In practice, we cannot meaningfully conduct this test with the current data set, since it would further remove data from the $l_u = l_*$ sample, which already yields formal errors on Ω_0 that span the allowed range, but do employ a similar technique below.

So far we have only discussed measurements of Ω_0 and c . Each curve, however, is also parameterized by an amplitude $a = h_0 \langle l \sin \phi \rangle_0$. If we assume functional forms for $P(l)$ and $P(\phi)$, as well as values for l_{\min} , l_* , and ϕ_u , we can compute the theoretical value of $\langle l \sin \phi \rangle_0$ in regions B and BC of Figure 3, given respectively by

$$\langle l \sin \phi \rangle_0 \text{ in } B = \frac{\int_{\phi'}^{\phi''} \left[\int_{l_1}^{l_{\max}} P(l) \langle l \sin \phi \rangle dl \right] P(\phi) d\phi + \int_{\phi_u}^{\phi''} \left[\int_{l_1}^{l_2} P(l) \langle l \sin \phi \rangle dl \right] P(\phi) d\phi}{\int_{\phi'}^{\phi''} \left[\int_{l_1}^{l_{\max}} P(l) dl \right] P(\phi) d\phi + \int_{\phi_u}^{\phi''} \left[\int_{l_1}^{l_2} P(l) dl \right] P(\phi) d\phi}, \quad (10)$$

$$\langle l \sin \phi \rangle_0 \text{ in } BC = \frac{\int_{\phi'}^{\phi_u} \left[\int_{l_1}^{l_{\max}} P(l) \langle l \sin \phi \rangle dl \right] P(\phi) d\phi}{\int_{\phi'}^{\phi_u} \left[\int_{l_1}^{l_{\max}} P(l) dl \right] P(\phi) d\phi}, \quad (11)$$

where $l_1 = l_{\min} \sin \phi_u / \sin \phi$, $l_2 = l_* \sin \phi_u / \sin \phi$, $\phi' = \arcsin(l_{\min} \sin \phi_u / l_{\max})$ is the minimum angle to the line of sight at which objects with intrinsic size l_{\max} can be seen by the survey, and similarly, $\phi'' = \arcsin(l_* \sin \phi_u / l_{\max})$. The denominators in equations (10) and (11) assure proper normalization. The best-fit values of $a = h_0 \langle l \sin \phi \rangle_0$ for $l_u = l_{\max}$ and $l_u = l_*$, can thus be compared with the theoretical value of $\langle l \sin \phi \rangle_0$ in regions BC and B , respectively, to arrive at values for h_0 in each

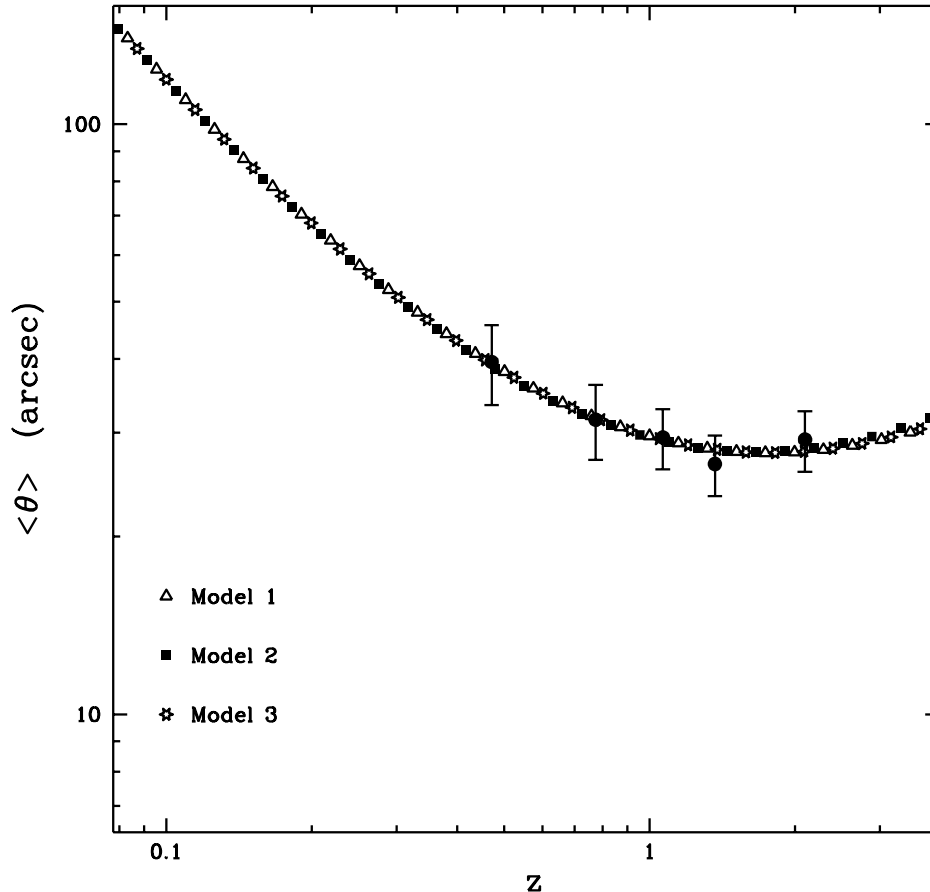


FIG. 6.—Best-fit results obtained with $l_u = l_*$ for models 1, 2, and 3. These Friedmann models all yield nearly identical values for a , c , and Ω_0 , so that their θ - z curves, traced by the different point styles in the figure, virtually overlap.

TABLE 6
RESULTS FOR H_0 IN $\text{km s}^{-1} \text{Mpc}^{-1}$ WITH 1σ
CONFIDENCE LIMITS

Model	Limit	H_0	
		($\phi_u = 45^\circ$)	($\phi_u = 90^\circ$)
1	l_{\max}	99 (59, 170)	62 (37, 107)
2	l_{\max}	107 (64, 174)	68 (41, 110)
3	l_{\max}	98 (64, 152)	62 (40, 96)
1	l_*	55 (36, 77)	39 (26, 54)
2	l_*	49 (33, 114)	35 (23, 81)
3	l_*	48 (32, 93)	34 (23, 66)

Friedmann model. Though not a valid determination of H_0 , this does offer a consistency check on our analysis, in the sense that we expect reasonable input assumptions to yield plausible values for H_0 .

If the lobe sizes grow as $l = vt$ with some expansion velocity v , and then fade, with an overall lifetime of about 10^7 – 10^8 yr (Nilsson et al. 1993; Neeser et al. 1995; Gopal-Krishna et al. 1996), a population of such objects observed over cosmological timescales $\gg 10^8$ yr will yield an observed distribution of sizes roughly constant between l_{\min} and l_{\max} . In this case, the normalized probability density between l_{\min} and l_{\max} is given by $P(l) = 1/(l_{\max} - l_{\min})$. For a spherically symmetric distribution of randomly oriented rods, $P(\phi) = \sin \phi$ for $0 < \phi < \phi_u$ (Harwit 1988, p. 111). If quasars are viewed at arbitrary projection angles, then $\phi_u = 90^\circ$. In the unified model, however, the jet axes of quasars tend to lie nearer to the line of sight, so that $\phi_u \approx 45^\circ$. We consider both values for ϕ_u . The theoretical value of $\langle l \sin \phi \rangle_0$ in region B also depends on l_{\min} , l_{\max} , and l_* , while that in region BC depends only on l_{\min} and l_{\max} . The ratios between these quantities, however, are determined by the data; points lying near $\theta_i(z)$ for a given model (from step 3 in our analysis method) were assumed to correspond to the maximally deprojected minimum intrinsic size, $l_{\min} \sin \phi_u/D_A$, while the uppermost points in the θ - z plane are taken to correspond to $l_{\max} \sin \phi_u/D_A$, so that the values of l_{\min}/l_{\max} are uniquely determined from the output data sets used to fit our Friedmann models. The ratio l_{\min}/l_* is also fixed from our requirement that the minimum in the θ - z curve arising from l_* be fixed at $65''$. To complete the theoretical calculation, it remains only to assume a value for l_{\max} , the present-day maximum intrinsic linear size. The largest known double-lobed radio sources have estimated intrinsic linear sizes of order 1 Mpc (A. Schoenmakers 1997, private communication). We thus take $l_{\max} = 1.2$ Mpc, which yields values of $l_{\min} \approx 70$ kpc for the various Friedmann models.

Our inferred results for H_0 under these assumptions, using all the observed data above the $12''$ survey limit, are shown in the top half of Table 6, along with the 1σ error ranges. The derived values for H_0 vary simply as $1/l_{\max}$. Though the error bars are considerable, the plausible assumptions we have made yield results for H_0 that agree generally with the range spanned by current measurements (Sandage & Tammann 1996; Kim et al. 1997; Falco et al. 1997; Holzapfel et al. 1997; Giovanelli et al. 1997; Schechter et al. 1997), with the unified model giving higher values. This in turn suggests that our model and input assumptions are in fact reasonable. It is also interesting to examine the derived values for H_0 using an upper limit to the data corresponding to l_* . Although the best-fit values of Ω_0 and c are different in this case, and the predicted theoretical value of $\langle l \sin \phi \rangle_0$ in region B differs from that in region BC , the best-fit value of a in each model, as determined by the l_* data, should compensate so as to yield values for H_0 , in agreement with the l_{\max} results, if the input assumptions are valid. The lower half of Table 6 shows that while the l_* values are systematically lower, they are consistent to within the 1σ errors with those obtained using l_{\max} . In particular, the range of values (in $\text{km s}^{-1} \text{Mpc}^{-1}$) for which the 1σ limits from identical models using limits of l_{\max} and l_* overlap are 59–77, 64–114, and 64–93, respectively, for models 1, 2, and 3, assuming $\phi_u = 45^\circ$, and 37–54, 41–81, and 40–66, assuming $\phi_u = 90^\circ$.

5. CONCLUSION

Using the FIRST radio survey and available redshift information, we have constructed a carefully defined set of double-lobed quasars whose observed θ - z relation, unlike those of many previous studies, appears to show evidence for curvature. We attribute this result to the precise sample definition, to the increased depth and sensitivity of the survey data, and to our self-consistent method of analysis, which addresses many of the problems associated with previous work in this area. We have explored the correlations between the intrinsic properties of these sources and find evidence, regardless of cosmological parameter values, for apparent size evolution arising from an inverse power-size correlation and evidence against intrinsic size evolution, both of which agree with the results of some previous authors. We find that while the present data can place interesting constraints on Ω_0 within a given cosmological model, in particular, suggesting, for models with $\Omega_0 \leq 1$, values in the range from 0.25 to 1.0 inclusive, with some evidence favoring values of (or near) unity, they cannot distinguish between various models with reasonable significance.

A larger data sample (e.g., from additional redshift information on the thousands of radio doubles in the FIRST survey), however, would place stronger constraints on the parameters within each model and may be able to distinguish among models. To investigate this, we have performed a Monte-Carlo simulation using $P(\phi) = \sin \phi$, $P(l) = 1/(l_{\max} - l_{\min})$, $l_{\max} = 1$ Mpc, $\phi_u = 45^\circ$, $H_0 = 50 \text{ km s}^{-1} \text{Mpc}^{-1}$, and an effective resolution cutoff at $12''$, to generate mock θ - z data for double-lobed sources assuming different cosmological models and choices of Ω_0 . We find that, if apparent size evolution is negligible, a data sample with ~ 500 points can recover the input value of Ω_0 to within ± 0.2 , but, in the case of underdense models, still cannot effectively distinguish between models with and without a cosmological constant (see Fig. 1). If apparent size evolution with $c = -1$ is included, at least twice as much data is required to achieve comparable results, because of the sensitivity of χ^2 to c .

Our sample, like all other θ - z studies to date, consists of double-lobed sources whose sizes are measured in the radio but whose redshifts were typically obtained in an optically selected fashion. Although we offer evidence, in § 2, as to why no serious selection effects are believed to be introduced by this mixing of optical and radio properties, a more desirable approach, in principle, would be to obtain redshift information for a complete and homogeneous sample of radio-selected double-lobed sources. One can further refine the sample by including only radio sources with symmetric and colinear triple structure (i.e., core + two lobes), thereby minimizing asymmetrical effects that might distort the apparent angular size, such as relative motion with respect to the IGM, and simplifying the problem of optical identification, since the positions of the central engines are well-determined a priori. We have selected a sample of such objects from the FIRST database (Buchalter et al. 1998) and matched these with the Automatic Plate Machine scans of the POSS plates (Irwin & McMahon 1992; Irwin, Maddox, & McMahon 1994) to produce a subset of radio triples having optical counterparts to the central source. This sample constitutes a set of several hundred radio-selected double-lobed sources complete to roughly $V = 20$. About 5% of these objects have been previously identified as radio galaxies or quasars, and fewer than 1% of these sources have known redshifts (NED), although many are expected to be substantially beyond $z = 1$, the estimated median redshift of the FIRST survey (Cress & Kamionkowski 1997). If complete redshift information were acquired for such a sample, the resulting data set would, more reliably than data with mixed optical and radio information, further our understanding of the intrinsic properties and evolution of double-lobed radio sources, the behavior of the IGM density as a function of redshift, and the quasar-radio galaxy unification issue, and, perhaps most important, be instrumental in determining the potential impact of angular size-redshift studies in cosmology.

We wish to thank Chelsea T. Wald for her help in compiling the data sample, as well as Alexandre Refregier, David Schminovich, Catherine Cress, Jacqueline Van Gorkom, and Kevin H. Prendergast for their numerous insightful comments and suggestions. We acknowledge support from the NSF (grants AST-94-19906 and AST-94-21178), IGPP/LLNL, DOE contract W-7405-ENG-48, the STScI, the National Geographic Society (grant NGS 5393-094), Columbia University, and Sun Microsystems. This research has made use of the NASA/IPAC Extragalactic Database (NED), which is operated by the Jet Propulsion Laboratory, California Institute of Technology, under contract with the National Aeronautics and Space Administration.

REFERENCES

- Barthel, P. D. 1989, *ApJ*, 336, 606
 Barthel, P. D., & Miley, G. K. 1988, *Nature*, 333, 319
 Becker, R. H., White, R. L., & Helfand, D. J. 1995, *ApJ*, 450, 559
 Buchalter, A., et al. 1998, in preparation
 Burn, B. J., & Conway, R. G. 1976, *MNRAS*, 175, 461
 Chyży, K. T., & Zieba, S. 1993, *A&A*, 267, L27
 Condon, J. J. 1988, in *Galactic and Extragalactic Radio Astronomy*, ed. G. L. Verschuur & K. I. Kellerman (New York: Springer)
 Condon, J. J., et al. 1996, *NCSA ADIL*, JC, 01C
 Conover, W. J. 1980, *Practical Nonparametric Statistics* (New York: Wiley)
 Cress, C. M., Helfand, D. J., Becker, R. H., Gregg, M. D., & White, R. L. 1996, *ApJ*, 473, 7
 Cress, C. M., & Kamionkowski, M. 1997, *MNRAS*, submitted
 Falco, E. E., Shapiro, I. I., Moustakas, L. A., & Davis, M. 1997, *ApJ*, 484, 70
 Fanaroff, B. L., & Riley, J. M. 1974, *MNRAS*, 167, 31P
 Giovanelli, R., Haynes, M. P., da Costa, L. N., Freudling, W., Salzer, J. J., & Wagner, G. 1997, *ApJ*, 477, L1
 Gopal-Krishna & Kulkarni, S. R. 1992, *A&A*, 257, 11
 Gopal-Krishna et al. 1996, *ApJ*, 463, L1
 Gregg, M. D., et al. 1996, *AJ*, 112, 407
 Harwit, M. 1988, *Astrophysical Concepts* (New York: Springer)
 Heckman, T. M., et al. 1992, *ApJ*, 391, 39
 Hes, R., et al. 1995, *A&A*, 303, 8
 Hewitt, A., & Burbidge, G. 1993, *ApJS*, 87, 451
 Holzapfel, W. L., Arnaud, M., Ade, P. A. R., Church, S. E., Fischer, M. L., Mauskopf, P. D., Rephaeli, Y., Wilbanks, T. M., & Lange, A. E. 1997, *ApJ*, 480, 449
 Hooley, A., et al. 1978, *MNRAS*, 182, 127
 Hough, D. H., & Readhead, A. C. S. 1989, *AJ*, 98, 1208
 Irwin, M., Maddox, S., & McMahon, R. G. 1994, *Spectrum*, 2, 14
 Irwin, M., & McMahon, R. G. 1992, *Gemini*, 37, 1
 Kapahi, V. K. 1985, *MNRAS*, 214, 19P
 ———. 1989, *AJ*, 97, 1
 Kellerman, K. I. 1993, *Nature*, 361, 134
 Kim, A. G., et al. 1997, *ApJ*, 476, L63
 Krauss, L. M., & Schramm, D. N. 1993, *ApJ*, 405, L43
 Lister, M. L., et al. 1994, *ApJ*, 427, 125
 Masson, C. R. 1980, *ApJ*, 242, 8
 Miley, G. K. 1971, *MNRAS*, 152, 477
 Neeser, M. J., et al. 1995, *ApJ*, 451, 76
 Nilsson, K., et al. 1993, *ApJ*, 413, 453
 Onuora, L. I. 1989, *Ap&SS*, 162, 343
 ———. 1991, *ApJ*, 377, 36
 Oort et al. 1987, *A&A*, 179, 41
 Orr, M. J. L., & Browne, I. W. A. 1982, *MNRAS*, 200, 1067
 Rector, T. A., Stocke, J. T., & Ellingson, E. 1995, *AJ*, 110, 1492
 Sandage, A., & Tammann, G. A. 1996, preprint
 Schechter, P. L., et al. 1997, *ApJ*, 475, L85
 Singal, A. K. 1988, *MNRAS*, 223, 87
 ———. 1993, *MNRAS*, 263, 139
 Ubachukwu, A. A. 1995, *Ap&SS*, 232, 23
 ———. 1996, *Ap&SS*, 236, 167
 Ubachukwu, A. A., & Onuora, L. I. 1993, *Ap&SS*, 209, 169
 Veron-Cetty, M. P., & Veron, P. 1996, *Quasars and Active Galactic Nuclei* (7th ed.; ESO Sci. Rep. 17)
 Wardle, J. F. C., & Miley G. K. 1974, *A&A*, 30, 305
 Weinberg, S. 1972, *Gravitation and Cosmology* (New York: Wiley)
 White, R. L., Becker, R. H., Helfand, D. J., & Gregg, M. D. 1997, *ApJ*, 475, 479
 Zirbel, E. L. 1996, *ApJ*, 473, 713